Novel hybrid biocomposites for tendon grafts: The addition of silk to polydioxanone and poly(lactide-co-caprolactone) enhances material properties, *in vitro* and *in vivo* biocompatibility

Behzad Shiroud Heidari [a,b,c], Emma Muiños Lopez [d], Emma Harrington [a,b], Rui Ruan [e], Peilin Chen [e], Seyed Mohammad Davachi [f], Benjamin Allardyce [g], Rangam Rajkhowa [g], Rodney Dilley [a], Froilán Granero-Moltó [d], Elena M. De-Juan-Pardo [a,b], Minghao Zheng [e,h], Barry Doyle [a,b,c,*]

[a] *Harry Perkins Institute of Medical Research, QEII Medical Centre, Nedlands and the UWA Centre for Medical Research, The University of Western Australia, Perth, Australia*
[b] *School of Engineering, The University of Western Australia, Perth, Australia*
[c] *Australian Research Council Centre for Personalised Therapeutics Technologies, Australia*
[d] *Cell Therapy Area, Centro de Investigación Médica Aplicada, IDISNA, Universidad de Navarra, Pamplona, Spain*
[e] *Centre for Orthopaedic Research, Faculty of Health and Medical Sciences, The University of Western Australia, Perth, Australia*
[f] *Department of Biology and Chemistry, Texas A&M International University, Laredo, TX, USA*
[g] *Institute for Frontier Materials, Deakin University, Geelong, VIC, 3216, Australia*
[h] *Perron Institute for Neurological and Translational Science, Nedlands, Western Australia, Australia*

ARTICLE INFO

ABSTRACT

Biopolymers play a critical role as scaffolds used in tendon and ligament (TL) regeneration. Although advanced biopolymer materials have been proposed with optimised mechanical properties, biocompatibility, degradation, and processability, it is still challenging to find the right balance between these properties. Here, we aim to develop novel hybrid biocomposites based on poly(*p*-dioxanone) (PDO), poly(lactide-co-caprolactone) (LCL) and silk to produce high-performance grafts suitable for TL tissue repair. Biocomposites containing 1–15% of silk were studied through a range of characterisation techniques. We then explored biocompatibility through *in vitro* and *in vivo* studies using a mouse model. We found that adding up to 5% silk increases the tensile properties, degradation rate and miscibility between PDO and LCL phases without agglomeration of silk inside the composites. Furthermore, addition of silk increases surface roughness and hydrophilicity. *In vitro* experiments show that the silk improved attachment of tendon-derived stem cells and proliferation over 72 h, while *in vivo* studies indicate that the silk can reduce the expression of pro-inflammatory cytokines after six weeks of implantation. Finally, we selected a promising biocomposite and created a prototype TL graft based on extruded fibres. We found that the tensile properties of both individual fibres and braided grafts could be suitable for anterior cruciate ligament (ACL) repair applications.

1. Introduction

Native tendons and ligaments (TL) are frequently subjected to tension applied by muscular contraction or other external forces. Hence, ductility, flexibility, and load-bearing properties are critical for artificial tendon scaffolds. Biopolymers play a significant role in TL tissue repair, whether the treatment relies on tissue engineering strategies or using artificial TL grafts. The biopolymer chosen for the TL graft governs the mechanical properties, biocompatibility, and absorption rate of the scaffold. Synthetic polymers are often chosen for such applications because of the level of control over mechanical properties, degradation rate, and easy reproducibility with large-scale production. Alternatively, natural biopolymers such as proteins are often favoured because of their high degree of scaffold-tissue compatibility due to the positive biological

recognition of their chemical make-up [1].

In recent years, different hybrid biocomposites based on natural and synthetic biopolymers have been developed to achieve the optimal balance between the materials' properties for the fabrication of functional scaffolds. Poly(ε-caprolactone) (PCL), polylactide (PLA) and poy (lactic-co-glycolide) (PLGA) are the most common synthetic biopolymers blended with natural biopolymers, mostly collagen and gelatine, to promote biocompatibility and biofunctionality of TL scaffolds [2–5]. For instance, PLLA/collagen blends (PLLA/Coll-75/25, PLLA/Coll-50/50) were prepared and used to fabricate electrospun tendon scaffolds [6]. PLLA/Coll-75/25 showed more desirable mechanical properties after incubation in PBS for 14 days, compared to the PLLA/Coll-50/50 [6]. PCL/collagen and PLA/collagen were co-electrospun to create a scaffold for the tissue engineering of muscle-tendon junctions (MTJ), where the collagen greatly improved biocompatibility and provided suitable mechanical properties matched with the native MTJ [5]. Gelatine was also blended with PCL to promote proliferation, adhesion and tenogenic differentiation of fibroblasts *in vitro* [7,8]. Furthermore, it was shown that tendon scaffolds made of PCL/gelatine could support the regenerated tissue of injured patellar tendons to restore biomechanical strength in a rabbit model [8]. Most of those composites have been developed by mixing materials in a solvent, mainly because solution electrospinning is an accessible method for TL scaffold fabrication [9].

Silk, as a natural biopolymer, is a promising candidate to blend with synthetic biopolymers for tissue regeneration applications [10]. *In vitro* and *in vivo* experiments have indicated that silk proteins show a broad spectrum of benefits such as mechanical properties, slow degradation, low toxicity, the low/absence of immunoreactivity, and the possibility to functionalize silk proteins with cell-adhesion domains [11–13]. As a result, silk has been widely used in TL tissue engineering [14–17]. For example, a composite of PCL and silk fibrous scaffold containing a cell-laden hydrogel was developed for ligament regeneration with improved cell delivery and infiltration [14]. Silk fibres were also used to braid hierarchical scaffolds for anterior cruciate ligament (ACL) regeneration in a sheep model [15]. Hence, adding silk to synthetic biopolymers can help achieve the optimal balance between biocompatibility, biodegradation and mechanical properties [10,18].

Recently, we developed biocompatible blends based on poly(*p*-dioxanone) (PDO) and poly(L-lactide-co-ε-caprolactone) (LCL) copolymer with mid-term degradation rate and high elongation at break. The toughness of these PDO/LCL blends facilitate their use in applications such as TL scaffolds or suture applications. Blend containing a minority of PDO (10%–30%) resulted in small immiscible PDO droplets uniformly dispersed within the LCL matrix and demonstrated excellent *in vitro* cellular properties and toughening behaviour with a notable strain-hardening effect [19].

In this work, we aim to improve the properties of PDO/LCL blend, such as biocompatibility, toughness, and blend miscibility, by adding degummed silk and perform preliminary assessment of PDO/LCL/Silk as a suitable biocomposite for TL tissue engineering. PDO/LCL/Silk biocomposites are characterized by different imaging and mechanical testing techniques, and both *in vitro* and *in vivo* biocompatibility experiments investigated the effect of silk in the PDO/LCL blend. Finally, the processability and mechanical properties of a candidate PDO/LCL/Silk biocomposite was compared to a PDO/LCL blend by prototyping fibres and grafts suitable for ACL repair.

2. Materials and methods

2.1. Silk fibroin preparation

Silk cocoons were purchased from silk production centres in Northeast India. The cocoons were degummed as described previously [20]. Briefly, cocoons were degummed in a commercial dying machine (Thies), with 2 g/L sodium carbonate and 0.6 g/L sodium dodecyl sulphate carbonate (Sigma-Aldrich). Degumming was carried out for 20 min at 100 °C. Cocoons were then washed with warm distilled water followed by cold distilled water. The degummed fibres were then cut into snippets using a cutter mill, attritor milled and spray dried, following a previous study [21].

2.2. Biocomposite preparation

PDO/LCL/Silk composites were prepared by a solvent casting method at room temperature. LCL copolymer (L-lactide:caprolactone 75:25, $M_w = 430,000$ Da, BMG Inc) and PDO ($\eta_{inh} = 1.6$ dL/g, BMG Inc) were used to prepare the composites. First, LCL and PDO (PDO:LCL, 2:8) were added in *1,1,1,3,3,3*-hexafluoro-2-propanol (HFIP) to form 10 w/v % solution (P2L8 solution) using a magnetic stirrer at room temperature. After 30 min, when the polymers were partially dissolved in HFIP, 1–15% of silk powder was mixed with HFIP (half of the volume used for dissolving polymers) and stirred for 15 min at room temperature. Then, the silk solution was ultrasonicated at room temperature to improve silk dispersion uniformly through the HFIP. Then, the silk dispersion was gently added to the P2L8 polymer solution. The final PDO/LCL/Silk mixture was stirred for 12 h at room temperature until obtaining a homogenous solution. Finally, the homogenous mixture was poured into a glass Petri dish and placed in a fume hood for 24 h to evaporate HFIP. Residual solvent was removed by vacuum drying at 60 °C for 24 h and stored in a vacuum bag at 5 °C. The final thickness of films was ranged between 200 and 300 μm. Prepared composites were named P2L8-S"X" whereby "X" indicates silk fraction in composites containing 20% of PDO and 80% of LCL.

2.3. Material characterisation

Infrared spectroscopy was performed using a FTIR-ATR spectrometer (Polymer ID analyzer, PerkinElmer) with a 4 cm^{-1} resolution in the range of 400–4000 cm^{-1} for determining functional groups. Morphology of the composites before and after degradation was observed by scanning electron microscopy (SEM) (Zeiss 1555 VP-SEM) using platinum-coated samples at an accelerating voltage of 5 kV. The microscope was equipped with an energy dispersive X-ray spectrometry (EDS) unit for elemental analysis. Differential scanning calorimeter (DSC) analysis was performed (DSC 25, Discovery DSC Series, TA Instruments) under a nitrogen atmosphere with a heating rate of 15 °C min^{-1} from 20 °C to 200 °C. The melting temperatures (T_m) were recorded as the maximum of the endothermic peaks. The degree of crystallinity (X_c) expressed as a percentage was taken from the first heating run and calculated using Eq. (1):

$$X_c \ (\%) = \frac{\Delta H_m}{W_f \Delta H_m^\circ} \times 100 \tag{1}$$

Where, ΔH_m and W_f, respectively, are the enthalpy of melting and the weight fraction of each polymer, determined from DSC, and ΔH_m° is the enthalpy of melting for 100% crystalline polymer. ΔH_m° of PDO [22], PLLA [23] and PCL [23] are taken as 102.9, 93 and 81.6 J g^{-1}, respectively. Although there is no data available for melt enthalpy of PLLA-co-PCL, according to mixture law, ΔH_m° of LCL was calculated as 90.15 J g^{-1} based on the PLLA and PCL values.

Tensile failure properties of the composites were measured using miniaturized rectangular specimens with gauge length of 25 mm and width of 5 mm (based on type 5B in BS ISO 527: 2012) and an Instron universal tensile tester (Model 5969, Instron, High Wycombe, UK) equipped with a 500 N load cell. Toughness values were obtained by measuring the area under the stress-strain curve determined from tensile testing [24]. Tensile cyclic properties were studied on the rectangular specimens using Univert tester (Cellscale, Canada) equipped with a 200 N load cell. Ligaments are cyclically loaded during activities of daily living, resulting in peak ligament strain values of less than 4% [25].

Therefore, cyclic tests were performed over 5,000 cycles at 37 °C using a PBS bath during the whole test. Each cycle was programmed by stretching up to a strain of 5% within 5 s followed by recovering with the same speed (1%/s). For each PDO/LCL/Silk biocomposite, average results of five test specimens ($n = 5$) and three test specimens ($n = 3$) were reported for tensile failure and cyclic modes, respectively.

We used an atomic force microscope (AFM) to study the effect of silk on the surface roughness and micro-topography of the composites. The AFM (Keysight 5500 SPM, USA) was operated high resolution under contact mode and all measurements were taken at a scan rate of 1.22–2.3 lines per second at room temperature. The average roughness of the surface (R_a) was measured based on different random sites within a 10 μm × 10 μm area size, and we used Gwyddion software (v2.55) to reconstruct the micro-topography into 3D [26].

Contact angle was measured in air atmosphere and room temperature, using Ossila contact angle goniometer, to investigate the effect of silk on the hydrophilicity of the composites [19]. In addition, the surface energy of the blends was measured following ASTM D7490 using diiodomethane (3.0 μL) and DI water (9.0 μL). The surface free energy (γ_s) of each component of composites were calculated using Owens-Wendt method by dispersive and polar surface energy (γ^d and γ^p) with a set of test liquids on a solid surface based on Eq. (2), (3):

$$\gamma_s = \gamma_s^d + \gamma_s^p \tag{2}$$

$$\gamma_l(1 + \cos\theta) = 2\sqrt{\gamma_s^d \cdot \gamma_l^d} + 2\sqrt{\gamma_s^p \cdot \gamma_l^p} \tag{3}$$

Where s and l denote the solid and liquid surfaces, respectively, and the contact angle of a liquid droplet on the surface is shown by θ [27]. By obtaining γ_s for all the samples, the surface energy contrast was compared according to the composition.

The weight loss of samples was investigated during hydrolytic and enzymatic degradation. Specimens with $5 \times 5 \times 0.3$ mm³ surface area were prepared from the cast composite films and an initial dry weight measurement was recorded. For hydrolytic degradation, the specimens were immersed in PBS (pH 7.4) at 37 °C under slow shaking for 365 days. Enzymatic degradation experiments were carried out according to a previous method for silk-based nanocomposite films [28]. Under the enzymatic condition, the samples were incubated at 37 °C in PBS (pH 7.4) solution containing 1.0 U/mL Protease XIV (Sigma-Aldrich). Samples were incubated in enzyme solution for 56 days under slow shaking and the enzyme solution was replaced with a fresh solution every 3 days. At each time point, the samples ($n = 3$ per time point) were rinsed and gently blotted with a KimWipe® before being vacuum dried at room temperature for one day. Then, the remaining weight was measured, and the weight loss percentage was calculated based on the initial dry weight. A series of specimens were also collected for studying the degradation through SEM.

2.4. In vitro cell experiments

MTS assays were performed to quantify the number of metabolically active cells grown in the media according to a well-known protocol [29, 30]. Tendon-derived stem cells (TDSCs) isolated from mouse patellar tendon were seeded on the surface of composites in a 48-well plate ($5'10^3$ cells/well). Cells were cultured in minimal essential medium (MEM Alpha, Gibcoä) containing 10% fetal bovine serum (FBS, Gibcoä) and 1% streptomycin and penicillin mixture.

Culture plates were incubated at 37 °C in a humidified atmosphere of 5% CO_2. After 1 or 3 days of culture, MTS assay was performed to evaluate cell proliferation in the growth media. In accordance with the CellTiter®96 AQueous Non-Radioactive Cell Proliferation Assay kit (Promega, USA), [3-(4,5-dimethylthiazol-2-yl)-5-(3-carboxymethoxyphenyl)- 2-(4-sulfophenyl)-2H-tetrazolium (MTS)] was added to the media at planned time points and incubated in a dark room for 2 h at 37 °C, 5% CO_2. Optical density (OD_{490}) was measured in a 96-well plate

reader (Bio-Rad, Model 680, USA) for cell proliferation tests.

For confocal laser scanning microscope (CLSM) imaging, cells were fixed with 4% PFA for 15 min after 3 days of culture and washed with PBS after fixation. Cells were permeabilized with 0.1% Triton X-100 in PBS for 5 min at room temperature before being incubated with diluted Rhodamine phalloidin (ab235138; Abcam) (1/1000) in 0.2% BSA-PBS for 30 min at room temperature. Finally, cells were again washed with PBS before being mounted with Diamond Antifade Mountant and stored at −20 °C. CLSM was then performed using Nikon A1Si Microscope.

2.5. In vivo experiments

P2L8, P2L8-S3, and P2L8-S10 films are the selected groups to study the effect of silk in low and high contents *in vivo* biocompatibility. Circular samples (n = 5 per group) were punched (diameter = 5 mm; thickness = 200–300 μm) from the films. All samples were disinfected using 70% ethanol solution and then dried in a vacuum oven for 24 h at 70 °C followed by an exposition of the biomaterials to the UV light in a biosafety cabinet for 8 h prior to implantation.

All animal procedures were approved by Universidad de Navarra Animal Ethics Committee and Navarra regional Government (Protocol number CEEA 004–18). Thirty BALB/c(Ola) mice aged 7 weeks were obtained from Harlan. Mice were anesthetised using inhalation anesthesia, Isofluorane (ISOFLUTEK® 1000 mg/g; Karizoo), maintained in a ratio of 1.5–2% throughout the complete procedure. The anesthetised mice were shaved dorsally, and a 1 cm incision was performed at the lower back of mice to generate the subcutaneous space. Two samples from each group per animal were implanted in the right and left subcutaneous pocket space respectively. After the implantation, mice were housed in a barrier facility with a 24-h light/dark cycle. Mice were given *ad libitum* access to food and water and were sacrificed at 1 or 6 weeks after implantation (18 animals in total). At the respective final point, the implants were collected, including surrounding tissues, for histological and molecular analysis.

2.6. Histology and molecular analysis

The implants with surrounding tissues and capsules were washed in PBS and fixed in 4% PFA (PanReac, Barcelona, Spain) overnight for paraffin embedding following the previously described protocol [31–33]. Samples were dehydrated in graded ethanol and xylene, embedded in paraffin, and sectioned at a thickness of 4 μm. For histological evaluation, selected sections of the biocomposites implants were hydrated in decreasing graded ethanol and stained with Hematoxylin and Eosin to determine the level of fibrotic tissue and the presence of inflammatory cells. Immunofluorescence analysis was performed to specifically detect monocytes/macrophages using the primary antibodies of anti-F4/80 (ab6640; Abcam). Bright field digital images were acquired with an Aperio scan (Leica Biosystems) and fluorescence digital images with a Vectra Polaris Multispectral System (PerkinElmer).

For molecular analysis, the implants were washed in PBS and the total RNA extracted with TRIzol (Invitrogen) following the manufacture instructions. Briefly, 1 μg of RNA was retrotranscribed using qScriptTM Supermix (Quantabio). The qPCR was performed in a 7300 Real-time PCR machine (Applied Biosystems) using actin beta (*Actb*, Mm02619580_g1) as reference gene. Relative expression of the interleukine 6 (*Il-6*, Mm00446190_m1), Interleukine 1 beta (*Il-1β*, Mm02619580_g1) and interleukine 10 (*Il-10*, Mm01288386_m1) genes were calculated using the $2^{-\Delta\Delta Ct}$ method. All probes were purchased from Life Technologies.

2.7. Fibre and graft fabrication

Fibres of the biocomposites were fabricated using a 3D printer customised with a small pellet extruder (Bravo extruder, Polylab, Australia), as shown in Fig. S1. First, the cast films (thickness: 0.2–0.3

mm) were manually chopped into small flakes, approximately 4 mm × 4 mm, to feed the extruder. The fibre was extruded through a brass nozzle (diameter: 0.4 mm) and collected onto a 6.45 mm diameter rotating metal mandrel (12 rpm). The extrusion process was run by a G-code, where the extrusion speed (speed of internal screw) and temperature were 11.4 rpm and 190–193 °C, respectively. To prototype TL grafts from the biocomposites, seven fibres of each group were braided using a controlled hand-braiding technique, demonstrated in Fig. S1.

2.8. Statistical analysis

All data are presented as mean ± standard deviation (SD). For cell proliferation tests, a statistically significant difference between groups was accepted as $p < 0.05$ using Student's t-test. For molecular analysis, a statistically significant difference between groups was accepted as $p < 0.05$ using one-way ANOVA analysis followed up by the Tukey's Pos Hoc tests.

3. Results and discussion

3.1. Characterisations of biocomposites

3.1.1. Role of silk in morphological, thermal, and chemical properties

To investigate the morphology of the silk and its dispersion quality in PDO/LCL composites, SEM images were taken from the fractured cross-sections of samples (Fig. 1). The SEM image of P2L8 (Fig. 1A) shows a droplet-matrix morphology, indicating the blend is immiscible. The small droplets of PDO (<2 μm) are uniformly dispersed in the LCL matrix, which results in a high interfacial surface between the PDO and LCL matrix.

As shown in Fig. 1, the addition of silk into the polymeric matrix reduced the PDO droplet size, even in low concentrations of silk (e.g., P2L8-S1). Silk particles mainly ranged less than 10 μm (Fig. S2). The presence of silk particles (marked by yellow circles in Fig. 1) in the SEM images was grown by increasing the silk content. The dispersion of the silk particles (marked by yellow circles in Fig. 1) within the PDO/LCL matrix can be clearly observed in P2L8-S1 and P2L8-S3, while the silk agglomeration can be also seen in high contents of silk, particularly in P2l8-S15. The silk increased the miscibility between PDO and LCL by decreasing the size of PDO droplets. We postulate that the uniform size reduction of PDO droplets was influenced by a portion of silk, which was dissolved in HFIP and dispersed in the interface of PDO and LCL. Silk is composed of nitrogen groups due to the amino acid structure and the distribution of nitrogen groups, as found through EDS mapping (Fig. S3), demonstrates practically uniform dispersion of silk in the samples.

The effect of silk on the thermal properties and crystallinity of biocomposites was studied with DSC experiments, and the results are reported in Fig. 1A and B and Table 1. The melting temperature (T_m) and degree of crystallinity (X_c) of the neat PDO are 104.41 °C and 72.06%, respectively, compared to 152.56 °C and 18.14% for neat LCL. The polymeric chains in PDO are mostly arranged in crystalline lamellae causing the high crystallinity; however, the random incorporation of
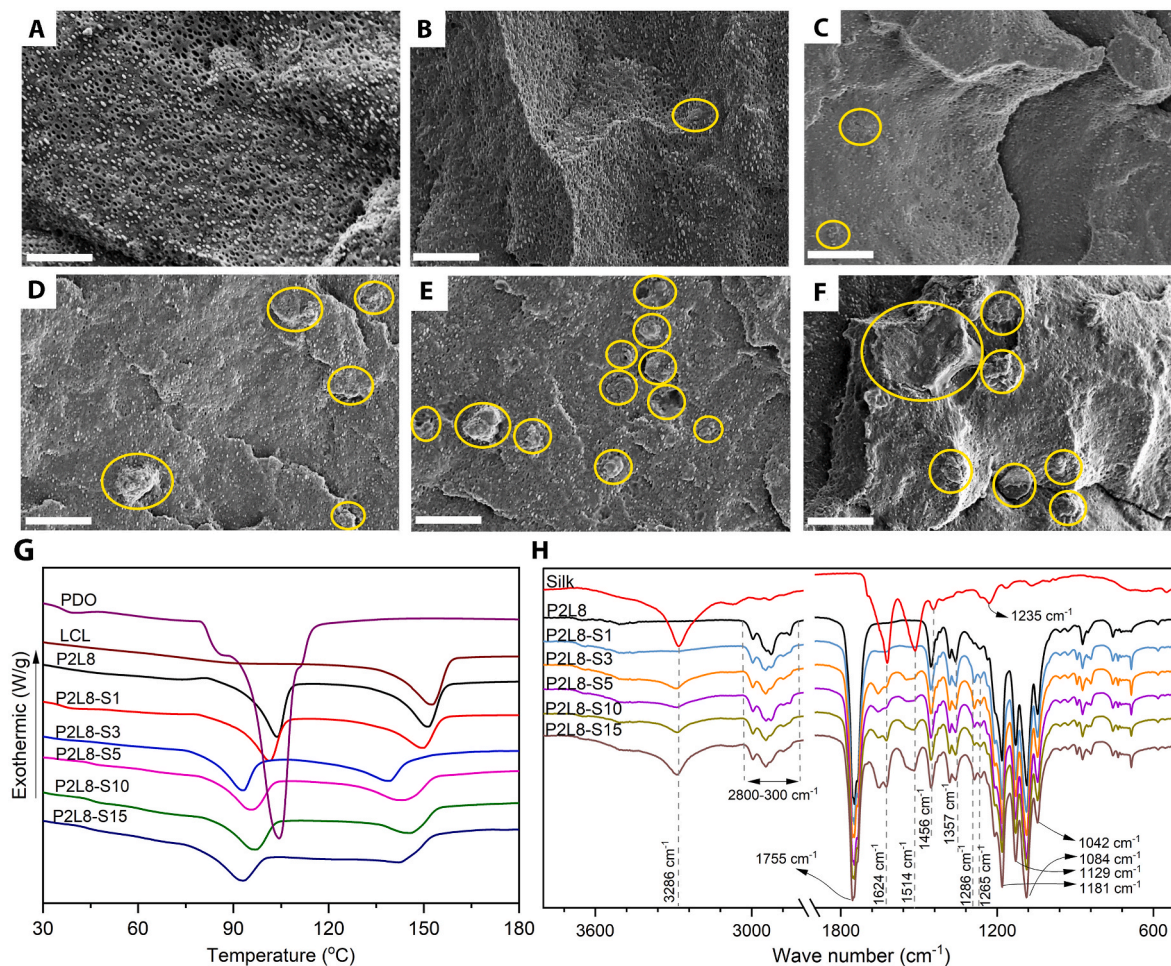
Fig. 1. Morphological and thermal properties of PDO/LCL/Silk composites. (A–F) SEM images of the fractured cross-sections of P2L8 (A), P2L8-S1 (B), P2L8-S3 (C), P2L8-S5 (D), P2L8-S10 (E), P2L8-S15 (F); scale bar = 10 μm; yellow circles show silk particles. (G) DSC diagrams. (H) FTIR spectra of silk and PDO/LCL/Silk composites.

Table 1
Melting temperature and crystallinity of PDO/LCL/Silk biocomposites.

Sample	PDO				LCL			
	T_m (°C)	ΔH_m (J g^{-1})	WHH (°C)	X_c (%)	T_m (°C)	ΔH_m (J g^{-1})	WHH (°C)	X_c (%)
PDO	104.41	74.16	9.46	72.06	–	–	–	–
LCL	–	–	–	–	152.56	16.36	12.59	18.14
P2L8	103.73	14.12	8.18	68.63	151.27	12.60	9.82	17.47
P2L8-S1	101.2	12.5	8.31	58.1	149.8	11.03	12.45	15.29
P2L8-S3	92.7	10.0	9.13	48.7	139.2	9.96	14.04	13.81
P2L8-S5	95.1	9.9	10.71	48.2	143.7	9.60	14.85	13.31
P2L8-S10	96.7	9.2	10.64	45.0	146.0	8.13	12.47	11.27
P2L8-S15	92.3	8.8	10.52	42.8	142.7	6.36	11.78	8.81

caprolactone units in the LCL restricted the movement of L-lactide units, resulting in low crystallinity in LCL [19,34]. P2L8 and all the silk composites showed two melting temperatures, indicating the successful mixing of the components and immiscibility of PDO and LCL phases. Blending PDO with LCL decreased the enthalpy of melting (ΔH_m) and X_c for both PDO and LCL phases since each polymer hinders the other polymeric chains' movement to fold and join the crystallisation growth front, resulting in a reduction in crystallinity in both phases [35].

From Fig. 1G and Table 1, adding silk up to 3% into P2L8 reduced T_m of composites, which shows the good dispersion and interfacial bonding of silk in the P2L8 matrix. However, the higher contents of silk, from 3% to 10%, increased the T_m for both phases because of the agglomeration of silk powder, which is in agreement with a previous observation of PLLA/PCL/Silk composites reported by Balali et al. [10]. Since we prepared the composites by a solution mixing method, the silk may present in the P2L8 matrix as dissolved silk, small-dispersed particles, and large agglomerates. The highest concentration of silk (15%) can saturate both polymer phases with dissolved silk in the presence of silk particles and agglomerates. Hence, we postulate that the reduction of T_m values in P2L8-S15 was due to the strong impact of saturated dissolved silk against the agglomerates. The crystallinity of PDO and LCL phases was constantly reduced by adding silk into P2L8 (Table 1), which was directly influenced by the reduction of ΔH_m. This reduction trend in X_c was mainly governed by the interfacial bonding and physical hindrance of the silk, which prevented the molecular movement of both PDO and LCL chains from full incorporation in the growth of crystalline lamella.

According to the width of the half-height crystallisation peak (WHH) (Table 1) a decrease of WHH for both PDO and LCL phases can be observed after blending 20% PDO with 80% of LCL (P2L8), indicating that each polymer increases the nucleation points in the matrix of the other polymer, leading to the increase in crystallisation rates [36,37]. However, the WHH of PDO and LCL showed an increasing trend in P2L8-S1, P2L8-S3, and P2L8-S5, meaning that the addition of silk decreases crystallisation rates up to 5% of silk content [10,38]. We know that plasticizers reduce nucleation points [39]; therefore, silk acts as a plasticiser and decreases the nucleation points in the polymer matrix, resulting in reduced crystallisation rates of both PDO and LCL phases [10]. WHH values, especially for LCL phase, were reduced in P2L8-S10 and P2L8-S15, showing an increase in crystallisation rates for the highest silk contents. On one hand, 10% and 15% of silk increase crystallisation rates; on the other hand, those amounts of silk decrease the degree of crystallinity (X_c) for both PDO and LCL phases. This means that the highest silk contents create many imperfect and restricted crystals within a short time frame as the silk agglomerates, limiting crystal growth.

Based on the thermal properties, there is a good dispersion and also reasonable interface bonding between P2L8 matrix and silk in the composites containing 1–5% of silk. However, P2L8-S10 and P2L8-S10 showed poor interface bonding and dispersion loses more energy and inhomogeneous thermal properties compared to enhanced interface bonding in the thermal processing of materials [40,41].

To evaluate chemical compositions, the FTIR spectra were recorded for PDO/LCL/Silk biocomposites, P2L8 blend and silk (Fig. 1H). In P2L8

blend, the sequential bands at 2800–3000 cm^{-1} are ascribed to $C–H$ stretching of $-CH_2$ groups in all samples [42,43]. The sharp peaks located at 1732 cm^{-1} are assigned to the carbonyl ($C{=}O$) stretching vibration of PDO and LCL (at 1755 cm^{-1}) at side chains. The peaks at 1042, 1084, 1129, and 1181 cm^{-1} belong to $C–O$ stretching vibration of PDO and the sequential peaks at 1456, 1383, and 1357 cm^{-1} represent the *-CH* bending vibration of PDO [37,42]. Hence, the spectra of P2L8 reflect the functional groups in both PDO and LCL, which were reported in our previous work [19]. The intensity and wave number of functional groups strongly depend on the ratio of PDO and LCL [19]. The spectrum of P2L8 is similar to the spectrum of LCL rather than PDO since the LCL is the dominant component in the blend.

Silk shows three absorption peaks at 1624 cm^{-1} (amide I), 1514 cm^{-1} (amide II), 1235 cm^{-1} (amide III), which are assigned with α-helix or random coil conformation, whereas the shoulder peak at 1441 cm^{-1} (amide II) and the peak at 1067 cm^{-1} (amide III) are attributed to β-sheet conformation [10,44]. Moreover, the broad band at 3286 cm^{-1} is due to the associating vibration hydroxyl *(-O-H)* group in the silk's chemical structure [10].

PDO/LCL/Silk biocomposites show a small shift in all the peaks, such as 1624 cm^{-1}, 1514 cm^{-1}, and 1235 cm^{-1}, compared to silk spectra. This can be an indication of the conformation transition in silk structure during solvent casting. The conformation transition was caused by the intermolecular hydrogen bonds formed by interactions between the hydroxyl groups of amino acids on the silk chain and the carbonyl groups of the esters, as previously reported for PLA/silk blend films [45]. Increasing the silk content in the biocomposites intensified the peaks related to silk's functional groups, particularly for amide I (1624 cm^{-1}), amide II (1514 cm^{-1}), and hydroxyl (3286 cm^{-1}) groups. However, no new peaks were found in the spectra of the biocomposite samples, indicating that no chemical reaction or functionalization occurred during the material preparation process.

3.1.2. Role of silk in mechanical properties

Tensile properties and example stress–strain curves of PDO/LCL/silk biocomposites are shown in Fig. 2A and Table 2, respectively. P2L8 shows a notable strain-hardening effect reaching ultimate strength of 18 MPa, 383% elongation at break and toughness of 55 MPa. The high elongation at break and toughening behaviour of P2L8 is caused by the uniform dispersion of small PDO droplets in LCL matrix. As previously reported, the small dispersed PDO droplets cause a high interfacial surface between the PDO and LCL matrix; as a result, the small droplets play a role in the load-bearing phase and decrease stress concentration in high elongations [19].

From Fig. 2A, silk changes the toughening behaviour of PDO/LCL/Silk biocomposites. Adding 1% of silk improves tensile strength (13%) and elastic modulus (78%), while the elongation at break (23%) shows a reduction, likely due to the strong interactions between silk and polymer matrix, stemming from reduced free-volume and restricted molecular mobility of the polymer chains. A similar reinforcing effect due to strong interactions between the particle and polymeric matrix was observed in other studies [10,23,27,46]. Conversely, adding 3% and 5% of silk reduces the elastic modulus (up to ~ -49.8%) and ultimate strength (up to
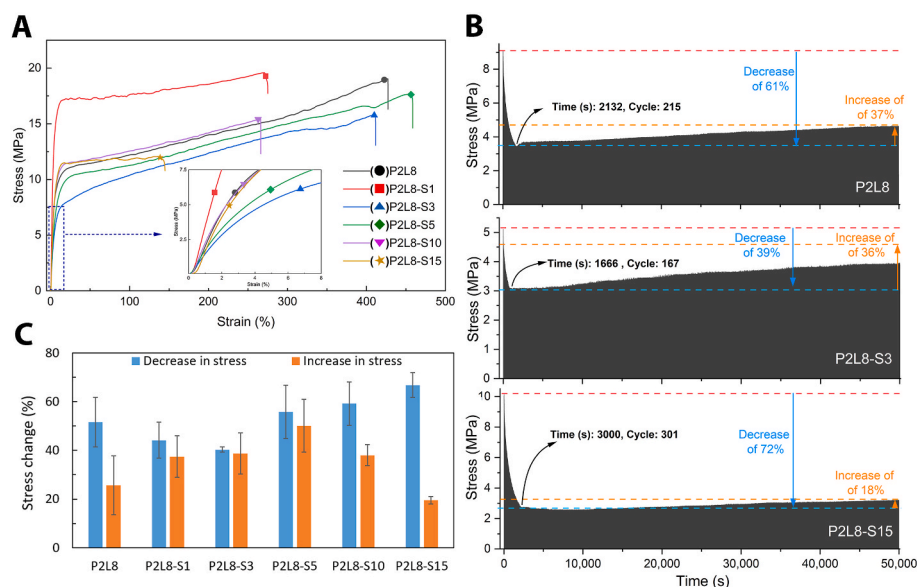
Fig. 2. Mechanical properties of PDO/LCL/Silk biocomposites. (A) Tensile stress–strain curves; (B) cyclic loading curves of P2L8 (top), P2L8-S3 (middle), and P2L8-S15 (bottom); (C) Changes of stress values (increase and decrease percentage) during cyclic loading tests.

Table 2
Tensile properties of PDO/LCL/Silk biocomposites. Reported values are shown as the mean ($n = 5$) ± standard deviation for mechanical properties.

Sample	Young's Modulus (MPa)	Ultimate strength (MPa)	Elongation at break (%)	Toughness (MPa)
P2L8	199.22 ± 20.40	18.03 ± 1.54	383.88 ± 68.36	54.91 ± 10.44
P2L8-S1	356.25 ± 44.21	20.33 ± 1.76	294.14 ± 44.23	50.70 ± 4.28
P2L8-S3	104.94 ± 28.81	14.94 ± 2.08	397.84 ± 88.37	54.86 ± 8.19
P2L8-S5	103.79 ± 16.85	16.55 ± 1.67	407.74 ± 37.98	52.79 ± 8.27
P2L8-S10	189.70 ± 33.34	14.73 ± 2.51	231.18 ± 73.91	29.38 ± 11.19
P2L8-S15	192.38 ± 26.99	11.84 ± 0.38	169.95 ± 38.17	20.86 ± 5.91

~ -16.8%) while increasing the failure strain (up to ~6.2%). The significantly improved elongation at break results from the uniform and much smaller dispersed PDO droplets in LCL matrix for P2L8-S3 and P2L8-S5 (Fig. 1E and F) compared to P2L8 and P2L8-S1 (Fig. 1C and D) [47]. This indicates that silk, in relatively low contents, softens the P2L8 blend, which could be influenced by the solution and distribution of a sufficient amount of silk inside the polymer matrix, and consequently, enhanced miscibility. The increased miscibility is supported by the cross-section SEM images of the biocomposites (Fig. 1) since the size of PDO droplets is reduced by adding silk, especially for those above 3% of silk. Such softening effect and reduction in elastic modulus were previously reported for other ternary blends in which one of the component compatibilized two immiscible polymeric phases by reducing the size of dispersed droplets [48].

However, high contents of silk, i.e. 10% and 15%, stiffen the biocomposites (elastic modulus up to ~190 MPa) again, while the ultimate strength and elongation at break decreased to 11 MPa and 169%, in P2L8-S15. This is confirmed by the silk agglomerates observed in P2L8-S10 and P2L8-S15 by SEM (Fig. 1G and H). The elastic modulus of a silk fibre, based on *B. mori* silk cocoons, could be up to 8.0 GPa, which is much higher than the modulus of P2L8 [13]; therefore, a high ratio of silk agglomerates caused higher stiffness, stress concentration, lower strain-hardening behaviour, and finally lower ultimate strength. As a

result, the toughness dropped from ~50 to 54 MPa (for 0–5% of silk) to ~20–30 MPa (for 10–15% of silk). A similar effect of a high ratio of agglomerates was reported in PLA/silk cast films [49], PLA/Silk electrospun membranes [50], and PLA/nanoperlite nanocomposite [27].

Cyclic loading is commonly used to investigate the fatigue response of materials. Since tendons are frequently subjected to tension loads applied by muscular contraction, it is important to choose an optimal biopolymer to fabricate loading-bearing tendon grafts. Fig. 2B illustrates the example cyclic stress-strain curves of P2L8, P2L8-S3 and P2L8-S15 over 50,000 s, equal to 5,000 cycles. The samples showed a sharp reduction in stress at the beginning, and then, a smooth constant increase in the pattern because of the stress-hardening behaviour of the biocomposites. Fatigue resistance can be evaluated by comparing the maximum decrease and increase in stress. For instance, there was a 39% decrease in maximum stress after 167 cycles for P2L8-S3, while P2L8-S15 decreased by 72% after 300 cycles (Fig. 2B). Fig. 2C shows the maximum decrease (%) and increase (%) of stress in the biocomposites. Adding silk up to 3% reduced the average stress decrease from 51.5% (P2L8) to 40.3% (P2L8-S3); however, loading 5–15% of silk elevated the average stress decrease to 66.7% in P2L8-S15. Conversely, the average maximum increase was improved from 25.6% in P2L8 to 50.0% in P2L8-S5, while adding more silk reduced the maximum increase to 19.5% in P2L8-S15.

The optimal fatigue resistance is assigned to minimum stress reduction (%) over cyclic loading. Furthermore, the stress growth, because of stress-hardening, could be beneficial in reinforcing the material over time. Given this, P2L8-S3 showed the best fatigue resistances among the biocomposites with ~40% and ~38% of maximum stress increase and decrease, respectively.

3.1.3. Role of silk in surface behaviour

Surface properties were studied using SEM, AFM images and contact angle measurements, and the surface morphology of the P2L8, P2L8-S3, and P2L8-S15 are shown in Fig. 3Ai-Aiii, respectively. Fig. 3Ai shows a smooth surface morphology of P2L8, while the presence of silk particles is clear on the surface of P2L8-S3 (Fig. 3Aii) and P2L8-S15 (Fig. 3Aiii), indicating the effect of silk on roughness at the macro-scale (i.e. overall surface). The silk particles were agglomerated on the surface of P2L8-S15 more than P2L8-S3, which corresponds with silk agglomeration in cross-section morphologies (Fig. 1A–F).

To further investigate the surface roughness at the submicron-scale,

3D topographic profiles (10 μm × 10 μm) and roughness analysis was obtained from the biocomposites' surfaces. The 3D topographic images of P2L8, P2L8-S3, and P2L8-S15 are represented in Fig. 3Bi-Biii. As can be seen, the addition of silk increased roughness, more significantly in P2L8-S15 (Fig. 3Biii), mainly due to silk agglomeration. In fact, the silk agglomerates created high variations in amplitude. The 3D topographic images agree with SEM images of the surfaces (Fig. 3Ai-Aiii) and for better comparison, quantified results are represented in Fig. 3C and Table 3. Average roughness (R_a) shows an increasing trend upon increasing the nanoparticle content. Up to 3% of silk, the roughness exhibits an insignificant difference (from 33.07 nm to 56.15 nm); however, when silk is increased to 5–15%, the roughness increases up to 254.4 nm. This suggests that high silk percentage creates surface roughness by the silk agglomerates. The maximum peak-to-valley height (R_t) (Table 3) also implicate the effect of silk agglomerates on surface roughness as the maximum heights increased sharply in the biocomposites containing more than 3% of silk. SEM and AFM images of other samples (P2L8-S1, P2L8-S5, and P2L8-S10) are displayed in Fig. S4.

Contact angle is influenced by the chemical nature of the polymer, surface roughness, surface heterogeneity, and surface energy type of the solvent used in the measurement and the crystallinity of the polymer [51]. The contact angle measurement with water and diiodomethane (DIM) is presented in Fig. 3D and Table 3. Water contact angles of P2L8 are measured at approximately 81°, which is slightly higher than the reported value for the PDO3LCL7 blend (containing 30% of PDO) in our previous study [19]. Contact angles reduced with increasing silk content, in both water and DIM. This indicates that the increase of silk improves hydrophilicity in the biocomposites, which could be affected by the chemistry of silk protein as well as surface roughness. On one hand, silk protein usually possesses a higher hydrophilic ability than polymers, because of its functional groups, resulting in changing the surface chemistry [52]. On the other hand, the increase of silk content produces surface roughness in the biocomposites; subsequently, increasing roughness leads to more hydrophilic surfaces (for surfaces showing water contact angles lower than 90°) as the water droplet wicks into the grooves on the surface [53,54].

Surface energies were calculated using water and DIM contact angles (Table 3); the results indicated increasing surface energy as SF content increased. This improvement is due to the presence of more hydrophilic silk on the surface of the biocomposites and is in agreement with the effect of silk on improved hydrophilicity of PCL/PLA/Silk composites, previously reported [10,55]. Therefore, adding silk particles into P2L8 improves the hydrophilicity and surface wettability of the blend, which could be beneficial in biocompatibility and cell attachment.

3.1.4. Role of silk in degradation

In vitro degradation investigations provide insight into possible degradation and erosion behaviour *in vivo*. Degradation of polymers can occur by the erosion, beginning with the cleavage of hydrolytic bonds leading to the formation of acidic by-products [56]. In this work, the acidic by-products were concentrated during degradation causing low pH values; however, these by-products are metabolised intracellularly or excreted human body during *in vivo* degradation [57]. Also, silk fibroin degrades *in vitro* and *in vivo* in response to proteolytic enzymes since silk is a protein-based biopolymer [58]. Hence, the degradation of the PDO/LCL/Silk biocomposites was investigated in both PBS (hydrolytic condition) and protease XIV (enzymatic condition) media over 365
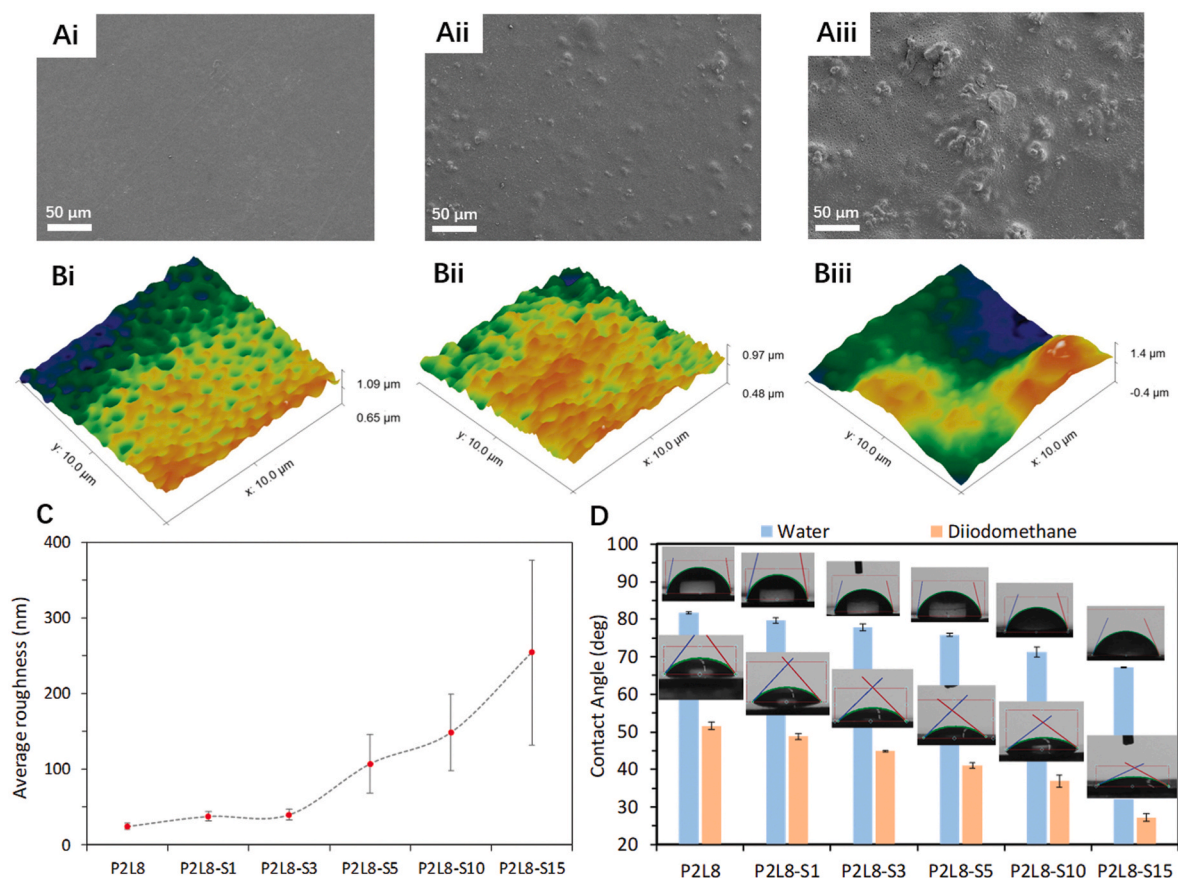
Fig. 3. Surface morphology, topography and hydrophilicity of PDO/LCL/Silk biocomposites. SEM image of the surface of P2L8 (Ai), P2L8-S3 (Aii), and P2L8-S15 (Aiii). AFM images of P2L8 (Bi), P2L8-S3 (Bii), and P2L8-S15 (Biii). (C) Average roughness of the surfaces obtained from AFM. (D) Water and diiodomethane contact angles.

Table 3

Surface roughness, contact angles, and calculated surface energies of the PDO/LCL/Silk biocomposites. Reported values are shown as the mean ($n = 3$) $\pm$ standard deviation for contact angles.

Sample	Average roughness (R_a, nm)	Maximum peak-to-valley height (R_t, nm)	Contact angle (deg)		Surface energy (mN/m)		
			Water	Diiodomethane (DIM)	γ_s	γ^d	γ^p
P2L8	24.72 ± 4.35	143 ± 25.58	81.7 ± 0.36	51.64 ± 0.96	33.43	27.83	5.60
P2L8-S1	37.97 ± 6.47	160.9 ± 30.42	79.59 ± 0.74	48.84 ± 0.79	35.05	28.85	6.19
P2L8-S3	56.15 ± 36.02	211.8 ± 31.94	77.74 ± 0.90	44.93 ± 0.23	37.17	30.43	6.43
P2L8-S5	107.3 ± 38.85	435.9 ± 160.7	75.85 ± 0.36	41.04 ± 0.76	39.20	32.44	6.76
P2L8-S10	148.8 ± 50.82	692.1 ± 197.8	71.32 ± 1.30	36.96 ± 1.64	41.58	32.75	8.82
P2L8-S15	254.4 ± 122.5	997.1 ± 336.4	67.07 ± 0.10	27.22 ± 0.95	45.88	36.02	9.86
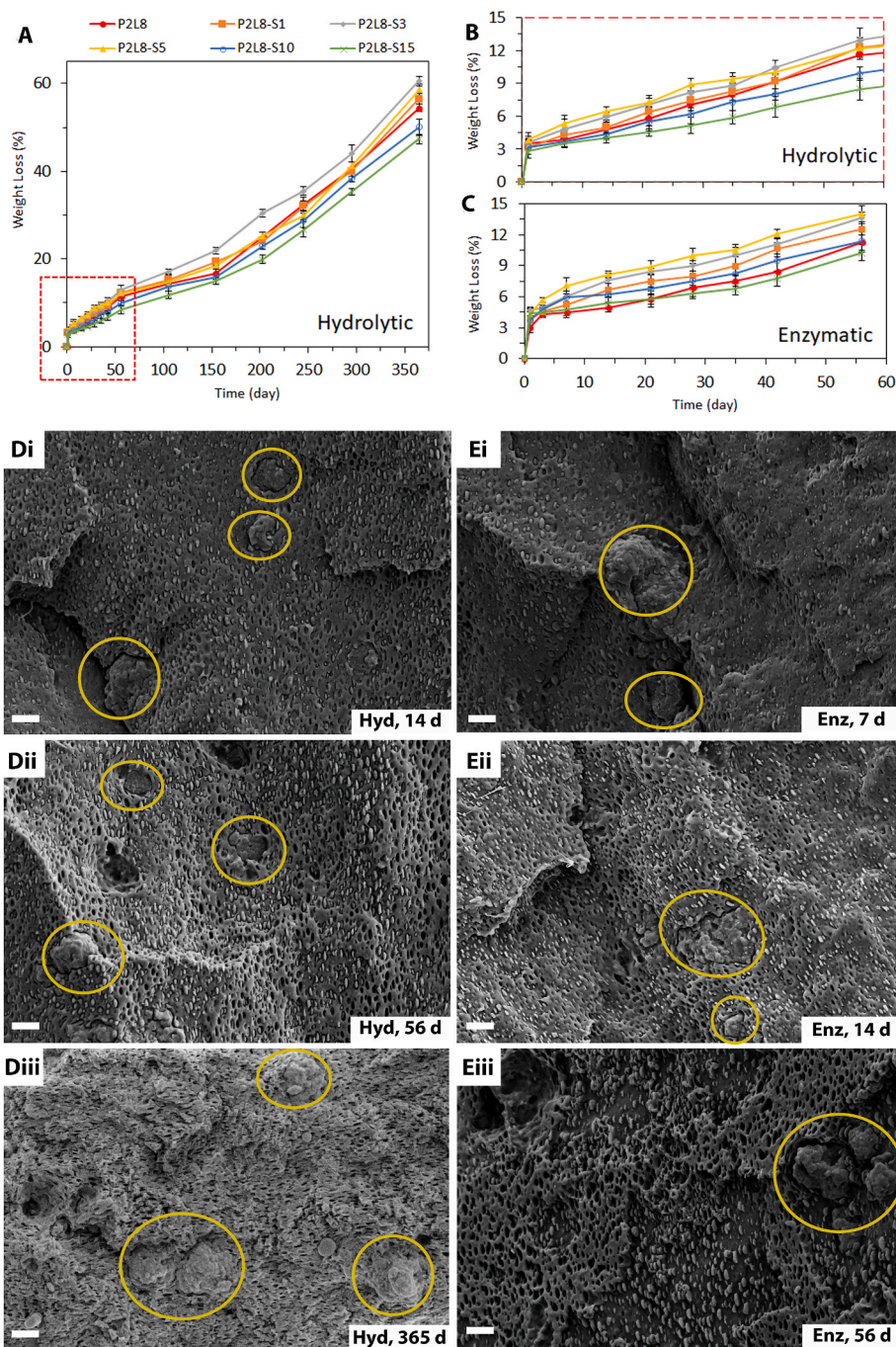
Fig. 4. Weight loss percentage of PDO/LCL/Silk biocomposites in hydrolytic (A, B) and enzymatic (C) degradations. SEM images of the fractured cross-sections of P2L8-S5 over hydrolytic (Di-Diii) and enzymatic (Ei-Eiii) degradation conditions; scale bar = 2 μm.

and 56 days, respectively.

Fig. 4A shows the weight loss (%) of the samples under hydrolytic degradation conditions over 356 days, while Fig. 4B and C illustrate the weight loss of the samples over 56 days in hydrolytic and enzymatic conditions, respectively. The addition of silk up to 3% increased the weight loss from 54.3% (P2L8) to 60.5% (P2L8-S3) after 365 days. This improved degradation is because of the silk's hydrophilicity and its effect on the structure of the biocomposites, such as cracking and surface erosion during degradation (SEM images shown in Fig. S5). Therefore, the silk enhanced water absorption, thus enabling more PDO and LCL hydrolysis by improving liquid penetration into the material [41]. Conversely, further loading of silk reduced the weight loss to 47.3% in P2L8-S15. This could be due to the slower degradation rate of silk than the polymers, especially PDO, which results in a reduction of the hydrolytic degradation rate of the biocomposites containing high silk contents. Silk is known as a non-degradable biomaterial in some products, like surgical sutures, because of its slow degradation [59]. Therefore, adding high contents of silk, like 15%, increases the incorporation of the slow-degradable portion inside the biocomposites. This agrees with the cross-section SEM images of P2L8-S5 during hydrolytic degradation shown in Fig. 4Di-Diii. As can be seen, silk particles are present inside the polymeric matrix in a similar size range after 14 days (Fig. 4Di), 56 days (Fig. 4Dii), as well as 365 days (Fig. 4Diii). In particular, the PDO droplets inside P2L8-S5 degraded almost completely after 365 days and a porous structure was left as a result (Fig. 4Diii), while the silk particles remain. This observation also suggests a higher hydrolysis rate of PDO than LCL, which is in agreement with previous studies [19,56,60].

As shown in Fig. 4B–C, there is no significant difference between the weight loss results obtained from hydrolytic and enzymatic conditions. After 56 days, P2L8 and P2L8-S1 showed around 11% and 12.5% weight loss, respectively, hydrolytically and enzymatically. However, the rest of the biocomposites showed slightly higher degradation rates in enzymatic than hydrolytic conditions. For instance, P2L8-S5 lost 14% of weight in enzymatic conditions, while 12.2% was recorded in hydrolytic conditions after 56 days. In fact, the enzymatic media contains protease which promotes silk protein degradation [28]. However, P2L8-S10 and P2L8-S15 showed lower degradation than P2L8 under enzymatic conditions. This could be related to the faster degradation of PDO than silk, as explained before. Thus, loading 10 or 15% of silk increases the incorporation of the slow-degradable portion inside the biocomposites.

Fig. 4Ei-**Eiii** shows the morphological changes of P2L8-S5 during incubation in the enzyme solution. Silk particles and PDO droplets are clear in the polymeric matrix after 4 days (Fig. 4Ei), 14 days (Fig. 4Eii), and 56 days (Fig. 4Eiii), indicating similar morphologies as observed in hydrolytic conditions over 56 days (Fig. 4Di-**Dii**). This means that enzymatic conditions cannot result in silk degradation significantly in bulk. However, the difference in surface morphology can be observed by comparing the surface erosion of P2L8-S5 after 56 days of incubation in PBS and protease XIV solution (SEM images shown in Fig. S6).

The degradability of silk has been demonstrated in different *in vitro* and *in vivo* models, revealing that the degradation rate can be effectively regulated by degumming, chemical treatment and source of silk [61,62]. For instance, Feng et al. [28] reported that the silk component significantly promotes the degradability of porous Silk/cellulose composite films in a protease XIV solution for 21 days. The difference between degradation results with this present work is the silk treatment, composite formulation, and physical structure. Future long-term studies *in vivo* studies will help reveal more information about the biodegradation of PDO/LCL/Silk composites in the extracellular matrixes of tissues that contain abundant proteases.

Biodegradation can significantly affect the mechanical performance of the biocomposites. PDO/LCL/Silk biocomposites degrade enzymatically and hydrolytically *in vivo*. The hydrolytic degradation may reinforce the biocomposites over the first few months because of the cleavage-induced crystallisation during hydrolytic degradation time.

We previously showed that the induced crystals over *in vitro* degradation increased the ultimate strength and modulus of PDO/LCL blends containing a minority of PDO [19]. However, the mechanical properties may reduce dramatically in the later stages of *in vitro* degradation because of the high brittleness of the biopolymers. In vivo degradation is normally faster than *in vitro* [63] and the reduction of mechanical properties *in vivo* conditions might be faster than *in vitro*. But it should be noted that the growth of tendon tissue during the resorption of the biocomposites can reinforce the TL grafts. Therefore, the effect of biodegradation on the mechanical performance of the biocomposites should be evaluated for the implanted scaffolds during TL regeneration in large animal models.

3.2. Biocompatibility of composites

3.2.1. In vitro cell experiments

Quantitative MTS results of proliferated active tendon-derived stem cells (TDSC) in the media are displayed in Fig. 5A. All biocomposites supported viable cell growth over 72 h of culture and were comparable with the positive control (a group without biocomposites). The addition of silk up to 3% enhanced proliferation; however, no further increase was observed in biocomposites containing 5–15%. Moreover, the statistical analysis, using Student's t-test, showed no significant difference (P > 0.05) between P2L8-S3, P2L8-S5, P2L8-S10, P2L8-S15 after 72 h of culture. In addition, the pure silk promoted the proliferation of TDSCs in the medium; however, the biocomposites containing 3–15% of silk showed much better results with significant differences (P < 0.05). This could be due to the high solubility of silk since it can change the concentration and composition of the cell culture medium containing 10% fetal bovine serum. Although the pH of silk solutions ranged between 7.5 and 7.7 in this study, the changes in supplements' concentrations in the medium can significantly affect the cells' survival, proliferation and/or differentiation [64]. Similar observations were reported in the other studies wherein the hybrid biocomposites, such as PVA/silk [65], PLLA/silk [66,67], PCL/silk [68], and LCL/silk [69], showed higher cell proliferations than pure silk samples.

CLSM and SEM imaging were used to display the adhered cells on the surface of the representative samples after 72 h, including P2L8 (Fig. 5Bi, 5Bii), P2L8-S3 (Fig. 5Ci, 5Cii), P2L8-S5 (Fig. 5Di, 5Dii) and P2L8-S15 (Fig. 5Ei, 5Eii). CLSM images (Fig. 5Bi-Ei) show the cytoskeleton of the attached TDSCs. A similar observation was found in CLSM and SEM images of P2L8-S1 and P2L8-S10 (Fig. S7). All the samples' surfaces support adherence and retention of cells throughout the experiment and the cell growth. An increased cell spreading was found in the samples containing silk compared to P2L8. Furthermore, SEM images confirmed the attached cells on the surfaces of P2L8 (Fig. 5Bii), P2L8-S3 (Fig. 5Cii), P2L8-S5 (Fig. 5Dii) and P2L8-S15 (Fig. 5Eii), which are in correspondence with CLSM images.

From our surface behaviour studies (Section 3.1.3), we found that silk improved the attachment and proliferation of TDSCs through different mechanisms linked to improved hydrophilicity in the biocomposites. This enahanced hydrophilicity could be due to both the chemistry of silk protein and the surface roughness of the biocomposite. In general, enhancing the hydrophilicity of a polymer surface results in better cell adhesion; however, polymer surfaces of super-hydrophilicity (contact angle below 5°) are not favourable to cell attachment and growth [70,71].]. The chemistry of silk protein plays a significant role in promoting cell attachment and proliferation. The fibroin protein in silk has a unique β-sheet structure containing amino acids groups, which provides signaling cues to the cells. As a result, silk fibroin has been considered as promising raw biomaterial to fabricate 3D scaffolds mimicking extracellular matrix (ECM) [72–75]. Surface roughness enhances cell attachment by providing more interactions between the cells and the surface, but it can also have detrimental effects, such as increased mechanical stress on the cells if the surface is too rough. For instance, we previously showed the macro-roughness level in PDO

A
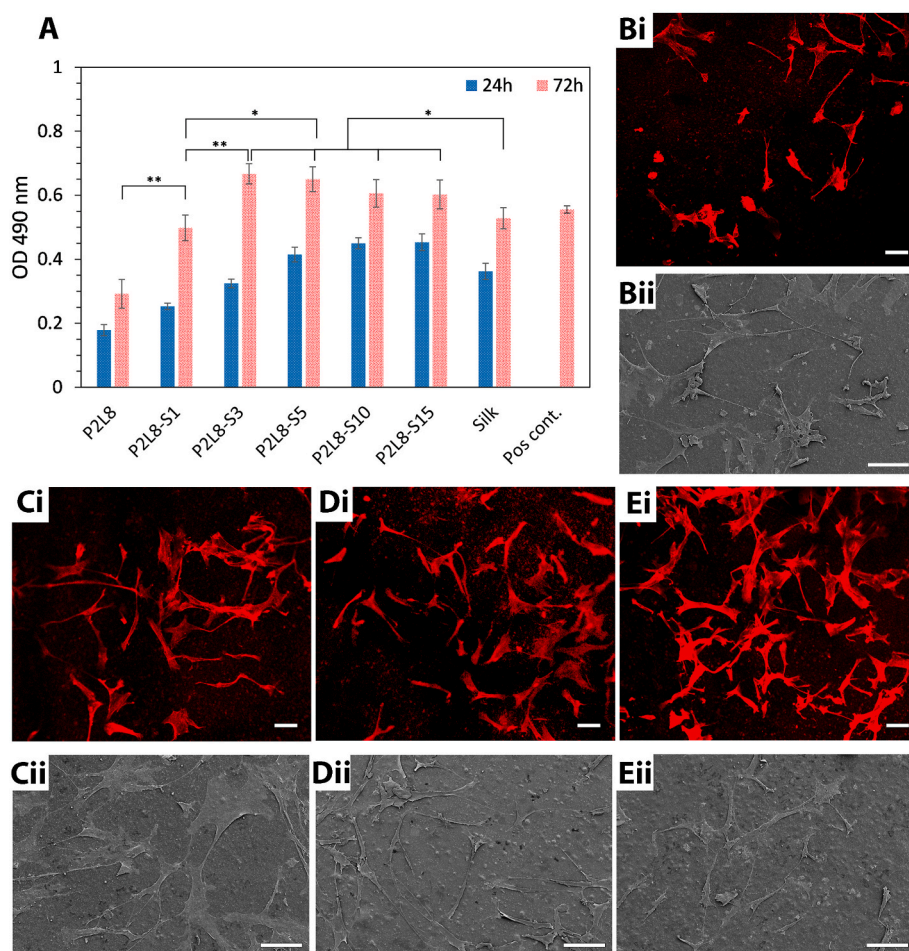
Fig. 5. Quantitative results of tendon-derived stem cells proliferation (A) by MTS test. (Bi–Ei) Fluorescence microscopy images of attached cells on the surface of P2L8 (Bi), P2L8-S3 (Ci), P2L8-S5 (Di), and P2L8-S15 (Ei) after 3 days culture. (Bii-Eii) SEM images of attached cells on the surface of P2L8 (Bii), P2L8-S3 (Cii), P2L8-S5 (Dii), and P2L8-S15 (Eii) after 72 h culture. Data are expressed as mean ± SD (n = 3). Statistical difference between groups is indicated ($*p < 0.05$; $**p < 0.01$). Scale bar = 100 μm.

isolated the fibroblast cells and hindered them from reaching each other [19]. In this study, a similar level of cell attachment can be found in the biocomposites containing 3–15% of silk; therefore, the increased roughness of biocomposites supports of TDSCs attachment to the surfaces. A similar observation was reported in previous studies, wherein the conjugation of silk fibroin to polylactic acid increased the hydrophilicity, and consequently, enhanced osteoblast cell attachment and proliferation [76,77].

3.2.2. In vivo experiments

In vivo studies using mice were conducted to understand the inflammatory response and foreign body reaction towards implanted P2L8, P2L8-S3, and P2L8-S10 films. Limited fibrotic tissue surrounded the biocomposites films after one and six weeks of implantation (Fig. S8). Histopathological analysis evaluated the local tissue response and H&E-stained sections displayed normal histology in all groups after one week and six weeks (Fig. 6). At week-one post implantation, there was no obvious acute inflammatory reaction found in the H&E staining in surrounding tissue in all samples (Fig. 6Ai-5Aiii). Moreover, after six weeks of implantation, no massive connective tissue was formed around the samples, suggesting that the acute and chronic inflammatory reactions are low (Fig. 6Ci-5Ciii).

As a key determinant of the inflammation process and a histopathological feature of chronic inflammation, the presence of macrophages was detected by F4/80 and immunofluorescence. All samples showed limited presence of macrophages after one week (Fig. 6Bi-5Biii), while P2L8 (Fig. 6Bi) the lowest presence of this immune population among the samples. After six weeks, P2L8-S3 (Fig. 6Dii) showed a slightly higher population of macrophages than P2L8 (Fig. 6Di) and P2L8-S10

(Fig. 6Diii), which was correlated to presence of inflammatory cell infiltration in the H&E staining (Fig. 6Cii). In summary, the results of F4/80 macrophage cells showed a very low acute and chronic inflammation of tissues surrounding the biocomposites film after one and six weeks.

Il-6, *Il-1β*, and *Il-10* are inflammatory cytokines typically secreted from activated macrophages, stimulating the inflammatory response and foreign body reaction towards the implanted materials. *Il-6* and *Il-1β* act to make disease worse (pro-inflammatory), whereas *Il-10* serves to reduce inflammation and is known as an anti-inflammatory cytokine [78]. As shown in Fig. 6Ei-Eiii, P2L8 kept a low expression of *Il-6* (Fig. 6Ei), *Il-1β* (Fig. 6Eii), and *Il-10* (Fig. 6Eiii) after one week of implantation. Moreover, all the samples showed a similar average expression of *Il-10* (around 1.8) and P2L8-S3 expressed the highest level of *Il-6* among samples.

The inflammatory response is influenced by the degradation rate of the biopolymers. The degradation by-products, like acidic breakdown fragments of the biopolymers, can decrease the pH of surrounding tissues and induce inflammatory reactions. Hence, the rate of degradation determines the local concentration of the acidic by-products [79]. In this work, the hydrolysis of the ester bond in LCL and PDO produces acidic by-products. We discussed that the degradation of P2L8 and the biocomposites occurred throughout the surface erosion followed by bulk erosion in the later stages. The incorporation of silk particles on the surface of the biocomposites can facilitate the surface erosion and release of polymeric fragments by creating several cracks on the surface (Figs. S5 and S6 in Supporting Information). Hence, the expressions of *Il-6* and *Il-1β* in P2L8-S3 and P2L8-S10 are slightly higher than P2L8 after one week of implantation.
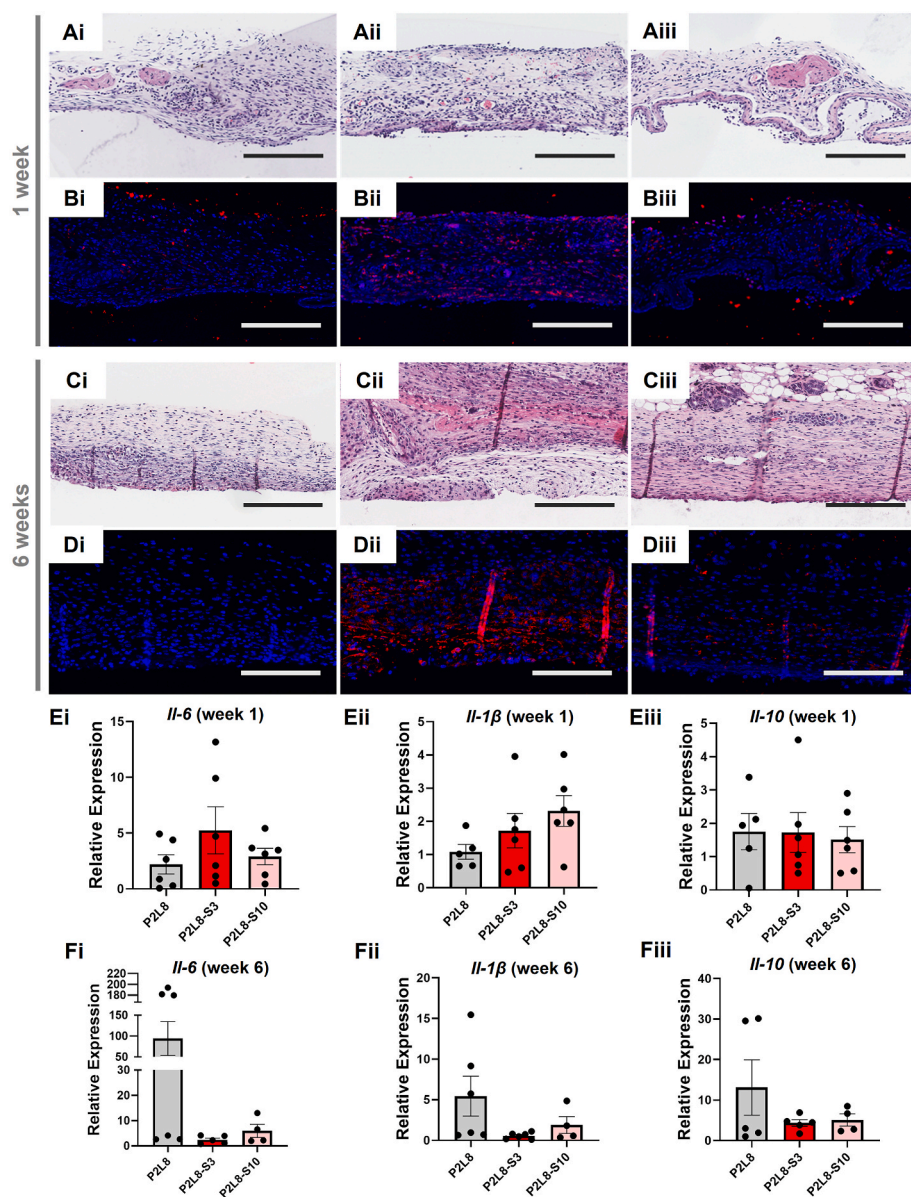
Fig. 6. Inflammatory responses associated with P2L8, P2L8-S3 and P2L8-S10 implants through histological and molecular analysis. H&E staining (Ai-Aiii) and F4/80 and immunofluorescent staining (Bi-Biii) sections of P2L8 (Ai, Bi), P2L8-S3 (Aii, Bii) and P2L8-S10 (Aiii, Biii) after one week. H&E staining (Ci-Ciii) and F4/80 and immunofluorescent staining (Di-Diii) sections of P2L8 (Ci, Di), P2L8-S3 (Cii, Dii) and P2L8-S10 (Ciii, Diii) after six weeks. Expressions of pro-inflammatory of cytokines including *Il-6, Il-1β, Il-10* after one (Ei-Eiii) and six (Fi-Fiii) weeks of implantation. There is no statistically significant difference between groups based on one-way ANOVA analysis followed up by the Tukey's Pos Hoc tests. Scale bar = 100 μm.

After six weeks the expression levels of *Il-6* (Fig. 6Fi), *Il-1β* (Fig. 6Fii), and *Il-10* (Fig. 6Fiii) were significantly increased in P2L8. In particular, the average expression of *Il-6* for P2L8 (Fig. 6Fi) was at least 10.0-fold higher than P2L8-S3 and P2L8-S10. This could be related to the higher concentrations of acidic by-products in P2L8 compared to biocomposites, due to the bulk erosion stage of degradation. In fact, the addition of silk in P2L8 blend can moderate the concentration of the by-products and slow down the autocatalytic degradation wherein the acidic by-products cause further increased degradation of remaining polymers [75]. Hence, the addition of silk reduced the expressions of pro-inflammatory cytokines after six weeks of implantation. The higher increased expression of *Il-10* in P2L8 shows a positive correlation between *Il-6* and *Il-10,* which indicates multiple cell types, such as monocytes, macrophages, and T-cells, counteracted the high inflammatory response and attempted to suppress inflammatory processes [80,81].

Our observation is in agreement with previous studies in which the expressions of inflammatory cytokines were diminished in PP, PCL and PVA after adding the purified silk to those polymers [82,83]. However, in the current study, there is no statistically significant difference between groups based on one-way ANOVA analysis followed up by the Tukey's Pos Hoc tests.

3.3. Fibres and grafts

Synthetic biopolymers and synthetic-based biocomposites are the most widely studied materials in TL and interface tissue engineering [1]. So far, we showed that the novel PDO/LCL/silk biocomposites offer improved tensile properties, degradation rate, *in vitro* and *in vivo* biocompatibility for TL tissue engineering applications. The important advantages of synthetic biopolymers are large-scale manufacturing, ease of processability, good mechanical properties, and controlled absorption in the human body [1,9]. Fibre extrusion in combination with the braiding/knitting technique is a well-known approach to creating micro- and nanofibrillar scaffolds with different alignment levels for tendon tissue engineering [1,9].

The addition of 3 and 5% of silk showed the best miscibility between PDO and LCL phases among the samples without major silk agglomeration through mechanical and morphological properties. Although P2L8-S5 showed the lowest average elastic modulus (103.7 MPa) among

the samples, it is close to the reported values of human ACL (111 MPa) [84,85]. In addition, P2L8-S5 showed the highest average strain at failure (407%) and excellent toughness (52 MPa). Hence, this composition was selected to compare against P2L8 in this section. P2L8 fibre (F–P2L8) and P2L8-S5 fibre (F–P2L8-S5) were extruded by a mini pellet extruder and collected onto a rotating mandrel as shown in Fig. 7Ai and 7Aii. After that, the fibres were braided to assemble grafts and demonstrate the biocomposite potential for TL repair applications.

The average diameter of the fibre (n = 5) was measured to be 360 ± 35 μm and 420 ± 42 μm for F–P2L8 and F–P2L8-S5, respectively. SEM images of F–P2L8 shows a smooth surface (Fig. 7Bi) with an oriented morphology along the fibre length because of the extrusion and pulling force of the mandrel on the molten fibre before the polymer cooled and solidified. In contrast, the surface of F–P2L8-S5 (Fig. 7Ci) possesses a roughness, with several oriented grooves and marks due to the added silk. The effect of extrusion is also clear in the cross-section morphology of the fractured F–P2L8 (Fig. 7Bii and 7Biii). As can be seen, the PDO droplets are oriented in a circumferential direction caused by a rotating screw compressing and melting the polymer as it is extruded through the nozzle. Hence, an immiscible droplet-matrix morphology can be observed for F–P2L8-S5, which is similar to the morphology of P2L8 cast film (Fig. 1A). We already showed that adding 5% of silk into P2L8 reduced the size of PDO droplets (Fig. 1D), meaning improved

miscibility between PDO and LCL phases. Similarly, the cross-section morphology of the F–P2L8-S5 (Fig. 7Cii and 7Ciii) indicates enhanced miscibility between PDO and LCL phases, compared to F–P2L8, due to silk particles. EDS mapping (Fig. S9) also confirmed the fine dispersion silk (nitrogen element) inside the polymeric blend.

Braiding is a common technique to improve the tensile strength of fibres and build TL grafts. Grafts based on F–P2L8 (G-P2L8) and F–P2L8-S5 (G-P2L8-S5) were fabricated through braiding seven fibres using a controlled hand-braiding technique. As seen in Fig. 7Di and Fig. 7Dii, the grafts achieved a regular pattern along the length of the braid. The tensile properties of fibres and grafts are represented in Fig. 8 and Table 4 in comparison with native ACLs. Fig. 8A displays the typical stress-strain curves of fibres and grafts of P2L8 and P2L8-S5. F–P2L8 showed higher average Young's modulus (Fig. 8B) and ultimate tensile strength (Fig. 8C) than F–P2L8-S5, which are in agreement with the results obtained for cast films (Fig. 2A). Hence, P2L8-S5 is softer than P2L8 in both cast film and fibre forms. Moreover, the average strain at failure of F–P2L8-S5 (408%) was higher than F–P2L8-S5 (302%) as shown in Fig. 8D. From Table 4, both F–P2L8 and F–P2L8-S5 showed higher modulus and tensile strength than their films (P2L8 and P2L8-S5). This indicates the extrusion process reinforced the material, which could be assigned to the pulling force of the mandrel resulting in the orientation of molten fibre before solidification, as confirmed by
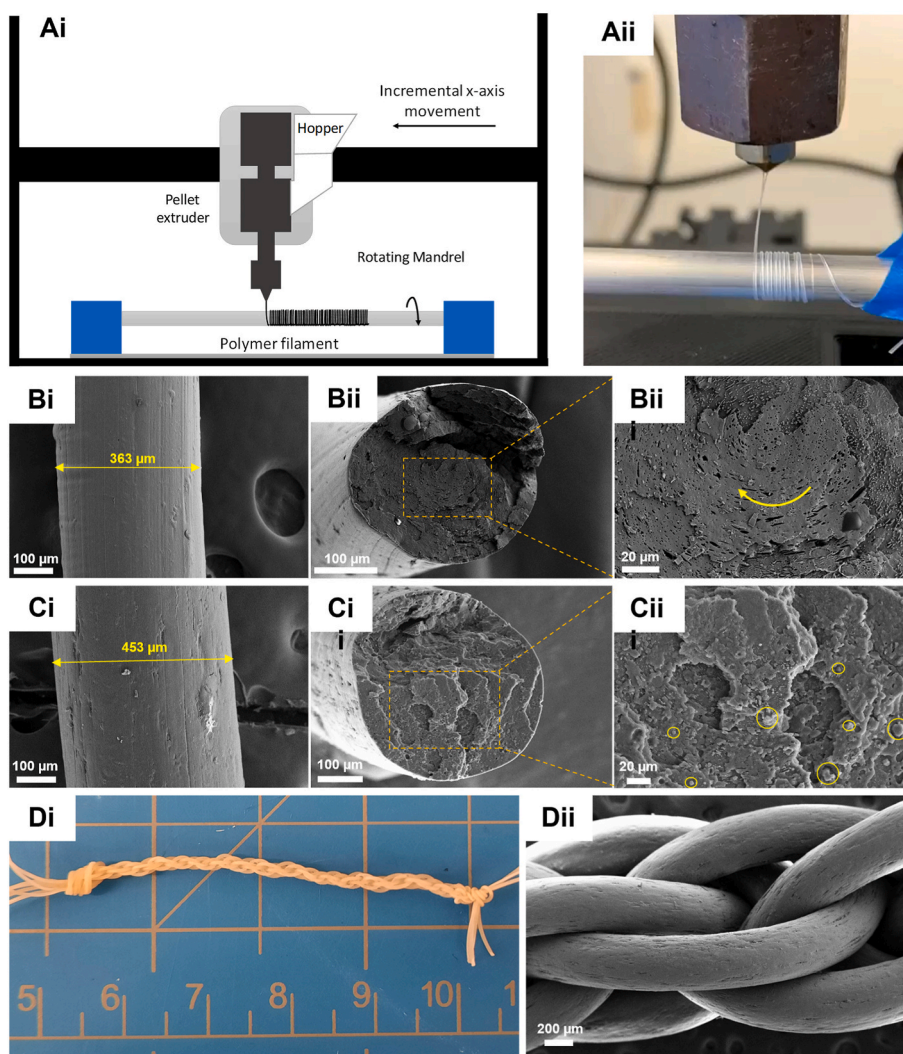
Fig. 7. (Ai) Schematic diagram of the set-up used in fibre fabrication. (Aii) Image of the collected fibre on the rotating mandrel. (Bi-Biii) SEM image of surface and fractured cross-section of F–P2L8. (Ci-Ciii) SEM image of surface and fractured cross-section of F–P2L8-S5. (Di-Dii) Demonstration of G-P2L8-S5 graft by a digit photograph and SEM image.
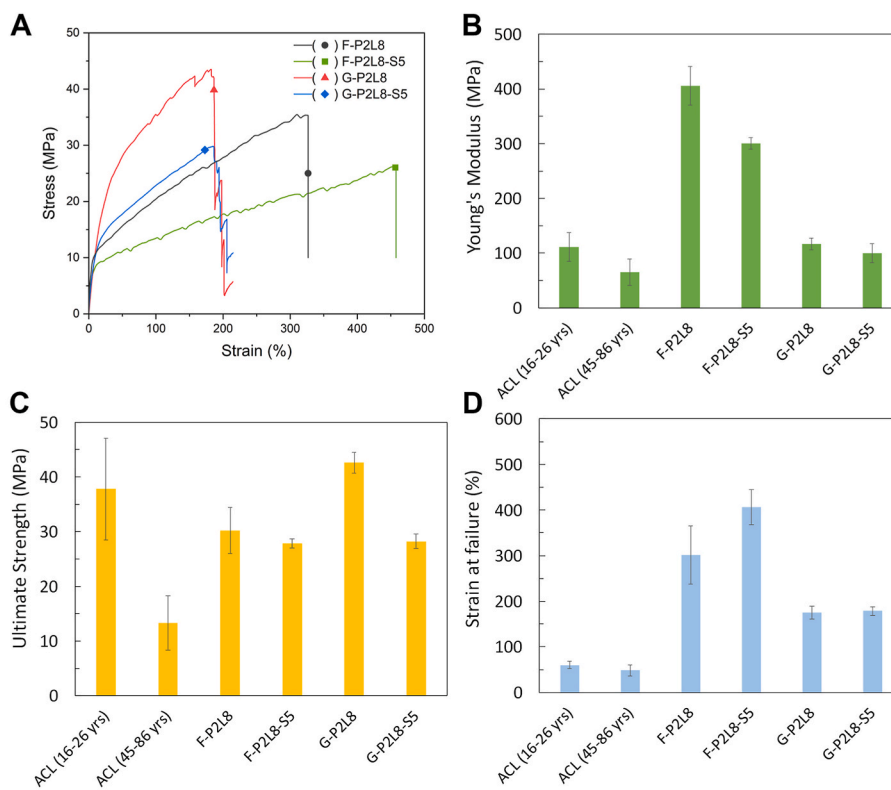
Fig. 8. (A) Tensile stress–strain curves of fibres and grafts. Young's modulus (B), ultimate strength (C), and strain at failure (D) of the fibres and grafts in comparison with human ACL properties [84,86].

Table 4
Tensile properties of films, fibres and grafts based on P2L8 and P2L8-S5. Mechanical properties are shown as the mean ($n = 5$) $\pm$ standard deviation.

Sample	Young's Modulus (MPa)	Ultimate strength (MPa)	Strain at failure (%)	Toughness (MPa)
P2L8	199.22 $\pm$ 20.40	18.03 $\pm$ 1.54	383.88 $\pm$ 68.36	54.91 $\pm$ 10.44
F–P2L8	405.49 $\pm$ 35.61	30.24 $\pm$ 4.20	301.75 $\pm$ 63.55	63.52 $\pm$ 15.82
G-P2L8	117.03 $\pm$ 10.66	42.59 $\pm$ 1.93	175.33 $\pm$ 13.69	57.24 $\pm$ 6.83
P2L8-S5	103.79 $\pm$ 16.85	16.55 $\pm$ 1.67	407.72 $\pm$ 37.96	52.79 $\pm$ 8.27
F–P2L8-S5	300.63 $\pm$ 10.7	27.89 $\pm$ 0.83	406.75 $\pm$ 38.00	75.26 $\pm$ 5.40
G-P2L8-S5	99.61 $\pm$ 17.39	28.23 $\pm$ 1.36	179.14 $\pm$ 9.44	38.68 $\pm$ 3.57
Human ACL (16–26 yrs) [84,86]	111 $\pm$ 26	37.8 $\pm$ 9.3	60.25 $\pm$ 6.78	10.3 $\pm$ 3.1
Human ACL (48–86 yrs) [84,85]	65.3 $\pm$ 24.0	13.3 $\pm$ 5.0	48.5 $\pm$ 11.9	3.1 $\pm$ 1.5

surface morphologies of the fibres in Fig. 7Bi and 7Ci. G-P2L8 and G-P2L8-S5 possess higher average ultimate strength than the relevant mono-fibres, indicating braiding enhanced the tensile strength. Strain at failure, however, was remarkably reduced after braiding. In addition, braiding reduced the average modulus of the fibres (approximately one-third), which shows that grafts are more flexible than fibres.

Synthetic biopolymer fibres have been previously used to fabricate tendon grafts [1,9]. For instance, Leroy et al. [87] prototyped tendon grafts for ACL repair using twisted/braided fibres of PLA-poloxamer/poloxamine copolymers. Although the average Young's

modulus of the extruded fibres (diameter: 140–210 μm) was reported as more than 2000 MPa, their yield strains were limited to 0.7–1.3%. Depending on polymer compositions, the tendon grafts showed average Young's modulus, yield stress, failure stress, yield strain and failure strains of 346–440 MPa, 19–21 MPa, 24–29 MPa, 5.4–6.4% and 20–78%, respectively [87]. Recently, PCL/gelatin microfibers were wet-spun with or without hydroxyapatite particles (HAp) to design tendon-to-bone interface gradient [3]. By varying the flow rates, wet-spun fibres could be obtained with diameters of 110–400 μm and Young's modulus in the range of 2.1–4.7 MPa for PCL/gelatin fibres and 0.6–0.7 MPa for PCL/gelatin/HAp fibres. However, no mechanical properties were reported for the tendon scaffold made by knitting (crochet) in that work [3].

Here, the tensile properties of the grafts are in the range of the properties of the human ACL. For instance, G-P2L8 showed a higher average modulus (117.0 MPa), tensile strength (42.6 MPa), and strain at failure (175.3%) than the reported values for ACL (16–86 years). Although the average ultimate tensile strength of G-P2L8-S5 (28.2 MPa) is lower than the average tensile strength (37.8 MPa) of the ACL in the ages (16–26 years), the actual tendon graft for human ACL repair could achieve higher strength by optimising spinning and braiding parameters such as the number of fibres, the diameter of fibres and braiding patterns. Therefore, the final graft for implantation could perform through controlled adsorption and a gradual decrease in mechanical properties over time.

4. Conclusion

In this work, novel biocomposite films based on PDO/LCL blend (P2L8) and silk fibroin (silk, 1–15%) were developed, characterized, and then used to prototype a tendon graft.

SEM images demonstrated that silk particles remained partially intact and dispersed throughout the biocomposites and increased the

miscibility between PDO and LCL phases, even when using low silk contents; this also reduces silk agglomerates seen at higher silk contents. The results of thermal properties and crystallisation behaviour of the composites indicated that the melting enthalpy and crystallinity of the biocomposites diminished upon the addition of silk because of the silk particle's effect on the polymeric chain movement of both PDO and LCL phases. The tensile properties showed that adding 3–5% of silk reduced the elastic modulus (up to ~100 MPa) and ultimate strength (up to ~15 MPa), while increasing the strain at failure (up to ~400%) because of the enhanced miscibility between PDO and LCL phases; confirmed by SEM imaging. All biocomposites containing up to 5% silk showed similar toughness and cyclic loading showed stress-hardening and reinforcing behaviour over time; P2L8-S3 exhibited the best fatigue resistance among the samples. Adding silk also increases the hydrophilicity, surface energy and roughness of the surfaces, and in contrast to high silk contents (10 and 15%), low silk contents (up to 5%) led to faster degradation of the biocomposites.

The incorporation of silk improves tendon-derived stem cell (TDSC) proliferation and attachment, with the surfaces of all biocomposites supporting cell growth. However, denser cytoskeleton networks were found in the samples containing silk compared to the neat P2L8. Furthermore, *in vivo* experiments revealed that adding silk to P2L8 minimises the expression of pro-inflammatory cytokines after six weeks of implantation in a mouse model. Finally, we also demonstrated the potential of the biocomposites as suitable tendon graft material and show that the tensile properties of braided grafts are in the range of human anterior cruciate ligament (ACL). Hence, they could be considered for tendon and ligament repair applications.

Overall, PDO/LCL/Silk biocomposites, containing up to 5% of silk particles, could be an attractive material for tendon/ligament repair applications. The resulting tendon/ligament graft could benefit from enhanced mechanical performance, good processability, excellent biocompatibility and a controlled adsorption rate, as well as optimisation through an advanced manufacturing process.

Funding

Acquisition: BHS, BJD, MZ.

CRediT authorship contribution statement

Behzad Shiroud Heidari: Conceptualization, Methodology, Formal analysis, Investigation, Writing – original draft, Writing – review & editing, Project administration, Funding acquisition. **Emma Muiños Lopez:** Methodology, Formal analysis, Investigation, Writing – review & editing. **Emma Harrington:** Methodology, Investigation, Writing – review & editing. **Rui Ruan:** Methodology, Formal analysis, Investigation, Writing – review & editing. **Peilin Chen:** Methodology, Formal analysis, Investigation, Writing – review & editing. **Seyed Mohammad Davachi:** Formal analysis, Writing – review & editing, Review. **Benjamin Allardyce:** Resources, Writing – review & editing. **Rangam Rajkhowa:** Resources, Writing – review & editing. **Rodney Dilley:** Methodology, Writing – review & editing. **Froilán Granero-Moltó:** Resources, Writing – review & editing. **Elena M. De-Juan-Pardo:** Writing – review & editing, Supervision. **Minghao Zheng:** Resources, Writing – review & editing, Supervision, Funding acquisition. **Barry Doyle:** Conceptualization, Resources, Writing – original draft, Writing – review & editing, Supervision, Project administration, Funding acquisition.

Declaration of competing interest

The authors declare the following financial interests/personal relationships which may be considered as potential competing interests: B. S.H. and B.J.D. are inventors on a patent application (PCT/AU2021/050782) titled "Biocompatible polymer compositions" submitted by The University of Western Australia that covers the material composition described in this work. The other authors have no conflicts of interest to declare.

Acknowledgement

Appendix A. Supplementary data

Supplementary data to this article can be found online at https://doi.org/10.1016/j.bioactmat.2023.02.003.

References

[1] B. Shiroud Heidari, R. Ruan, E. Vahabli, P. Chen, E.M. De-Juan-Pardo, M. Zheng, B. Doyle, Natural, synthetic and commercially-available biopolymers used to regenerate tendons and ligaments, Bioact. Mater. 19 (2023) 179–197, https://doi.org/10.1016/j.bioactmat.2022.04.003.

[2] A. Sensini, C. Gualandi, L. Cristofolini, G. Tozzi, M. Dicarlo, G. Teti, M. Mattioli-Belmonte, M. Letizia Focarete, Biofabrication of bundles of poly(lactic acid)-collagen blends mimicking the fascicles of the human Achille tendon, Biofabrication 9 (2017), 015025, https://doi.org/10.1088/1758-5090/aa6204.

[3] I. Calejo, R. Costa-Almeida, R.L. Reis, M.E. Gomes, A textile platform using continuous aligned and textured composite microfibers to engineer tendon-to-bone interface gradient scaffolds, Adv. Healthc. Mater. 8 (2019), https://doi.org/10.1002/adhm.201900200.

[4] S. Sahoo, S.L. Toh, J.C.H. Goh, A bFGF-releasing silk/PLGA-based biohybrid scaffold for ligament/tendon tissue engineering using mesenchymal progenitor cells, Biomaterials 31 (2010) 2990–2998, https://doi.org/10.1016/j.biomaterials.2010.01.004.

[5] M.R. Ladd, S.J. Lee, J.D. Stitzel, A. Atala, J.J. Yoo, Co-electrospun dual scaffolding system with potential for muscle-tendon junction tissue engineering, Biomaterials 32 (2011) 1549–1559, https://doi.org/10.1016/j.biomaterials.2010.10.038.

[6] A. Sensini, C. Gualandi, A. Zucchelli, L.A. Boyle, A.P. Kao, G.C. Reilly, G. Tozzi, L. Cristofolini, M.L. Focarete, Tendon fascicle-inspired nanofibrous scaffold of polylactic acid/collagen with enhanced 3D-structure and biomechanical properties, Sci. Rep. 8 (2018) 1–15, https://doi.org/10.1038/s41598-018-35536-8.

[7] S.J. Lee, H.J. Kim, M. Heo, H.R. Lee, E.J. Choi, H. Kim, D. Lee, R.L. Reis, S.H. Do, I.K. Kwon, In vitro and in vivo assessments of an optimal polyblend composition of polycaprolactone/gelatin nanofibrous scaffolds for Achilles tendon tissue engineering, J. Ind. Eng. Chem. 76 (2019) 173–180, https://doi.org/10.1016/j.jiec.2019.03.036.

[8] D. Sheng, J. Li, C. Ai, S. Feng, T. Ying, X. Liu, J. Cai, X. Ding, W. Jin, H. Xu, J. Chen, S. Chen, Electrospun PCL/Gel-aligned scaffolds enhance the biomechanical strength in tendon repair, J. Mater. Chem. B 7 (2019) 4801–4810, https://doi.org/10.1039/c9tb00837c.

[9] B. Shiroud Heidari, R. Ruan, E.M. De-Juan-Pardo, M. Zheng, B. Doyle, Biofabrication and signaling strategies for tendon/ligament interfacial tissue engineering, ACS Biomater. Sci. Eng. 7 (2021) 383–399, https://doi.org/10.1021/acsbiomaterials.0c00731.

[10] S. Balali, S.M. Davachi, R. Sahraeian, B. Shiroud Heidari, J. Seyfi, I. Hejazi, Preparation and characterization of composite blends based on polylactic acid/polycaprolactone and silk, Biomacromolecules 19 (2018) 4358–4369, https://doi.org/10.1021/acs.biomac.8b01254.

[11] A. Leal-Egaña, T. Scheibel, Silk-based materials for biomedical applications, Biotechnol. Appl. Biochem. 55 (2010) 155–167.

[12] L. Chambre, R.N. Parker, B.J. Allardyce, F. Valente, R. Rajkhowa, R.J. Dilley, X. Wang, D.L. Kaplan, Tunable biodegradable silk-based memory foams with controlled release of antibiotics, ACS Appl. Bio Mater. 3 (2020) 2466–2472, https://doi.org/10.1021/acsabm.0c00186.

[13] Y. Yao, B.J. Allardyce, R. Rajkhowa, C. Guo, X. Mu, D. Hegh, J. Zhang, P. Lynch, X. Wang, D.L. Kaplan, J.M. Razal, Spinning regenerated silk fibers with improved toughness by plasticizing with low molecular weight silk, Biomacromolecules 22 (2021) 788–799, https://doi.org/10.1021/acs.biomac.0c01545.

[14] J.H. Kim, Y.J. Choi, H.G. Yi, J.H. Wang, D.W. Cho, Y.H. Jeong, A cell-laden hybrid fiber/hydrogel composite for ligament regeneration with improved cell delivery

and infiltration, Biomed. Mater. 12 (2017), 55010, https://doi.org/10.1088/1748-605X/aa7b51.

[15] A. Teuschl, P. Heimel, S. Nürnberger, M. Van Griensven, H. Redl, T. Nau, A novel silk fiber-based scaffold for regeneration of the anterior cruciate ligament: histological results from a study in sheep, Am. J. Sports Med. 44 (2016) 1547–1557, https://doi.org/10.1177/0363546516631954.

[16] F. Bi, Y. Chen, J. Liu, Y. Wang, D. Xu, K. Tian, Anterior cruciate ligament reconstruction in a rabbit model using a silk-collagen scaffold modified by hydroxyapatite at both ends: a histological and biomechanical study, J. Orthop. Surg. Res. 16 (2021) 139, https://doi.org/10.1186/s13018-021-02281-0.

[17] S. Font Tellado, W. Bonani, E.R. Balmayor, P. Foehr, A. Motta, C. Migliaresi, M. Van Griensven, Fabrication and characterization of biphasic silk fibroin scaffolds for tendon/ligament-to-bone tissue engineering, Tissue Eng. 23 (2017) 859–872, https://doi.org/10.1089/ten.tea.2016.0460.

[18] C. Vyas, J. Zhang, Ø. Øvrebø, B. Huang, I. Roberts, M. Setty, B. Allardyce, H. Haugen, R. Rajkhowa, P. Bartolo, 3D printing of silk microparticle reinforced polycaprolactone scaffolds for tissue engineering applications, Mater. Sci. Eng. C 118 (2021), 111433, https://doi.org/10.1016/j.msec.2020.111433.

[19] B.S. Heidari, P. Chen, R. Ruan, S.M. Davachi, H. Al-Salami, E. de Juan Pardo, M. Zheng, B. Doyle, B.S. Heidari, A novel biocompatible polymeric blend for applications requiring high toughness and tailored degradation rate, J. Mater. Chem. B 9 (2021) 2532–2546, https://doi.org/10.1039/d0tb02971h.

[20] R. Rajkhowa, L. Wang, J.R. Kanwar, X. Wang, Molecular weight and secondary structure change in eri silk during alkali degumming and powdering, J. Appl. Polym. Sci. 119 (2011) 1339–1347, https://doi.org/10.1002/app.31981.

[21] R. Rajkhowa, L. Wang, J. Kanwar, X. Wang, Fabrication of ultrafine powder from eri silk through attritor and jet milling, Powder Technol. 191 (2009) 155–163, https://doi.org/10.1016/j.powtec.2008.10.004.

[22] A. Ahlinder, T. Fuoco, A. Finne-Wistrand, Medical grade polylactide, copolyesters and polydioxanone: rheological properties and melt stability, Polym. Test. 72 (2018) 214–222, https://doi.org/10.1016/j.polymertesting.2018.10.007.

[23] B. Torabinejad, J. Mohammadi-Rovshandeh, S.M. Davachi, A. Zamanian, Synthesis and characterization of nanocomposite scaffolds based on triblock copolymer of l-lactide, ε-caprolactone and nano-hydroxyapatite for bone tissue engineering, Mater. Sci. Eng. C 42 (2014) 199–210, https://doi.org/10.1016/j.msec.2014.05.003.

[24] W. Brostow, H.E. Hagg Lobland, S. Khoja, Brittleness and toughness of polymers and other materials, Mater. Lett. 159 (2015) 478–480, https://doi.org/10.1016/j.matlet.2015.07.047.

[25] B.C. Fleming, B.D. Beynnon, P.A. Renstrom, R.J. Johnson, C.E. Nichols, G.D. Peura, B.S. Uh, The strain behavior of the anterior cruciate ligament during stair climbing: an in vivo study, Arthrosc. J. Arthrosc. Relat. Surg. 15 (1999) 185–191, https://doi.org/10.1053/ar.1999.v15.015018.

[26] F.A. Jung, M. Schart, L. Bührend, E. Meidinger, J.J. Kang, B.J. Niebuur, S. Ariaee, D.S. Molodenskiy, D. Posselt, H. Amenitsch, C. Tsitsilianis, C.M. Papadakis, Highly tunable nanostructures in a doubly pH-responsive pentablock terpolymer in solution and in thin films, Adv. Funct. Mater. 31 (2021), 2102905, https://doi.org/10.1002/adfm.202102905.

[27] S. Toghi Aval, S.M. Davachi, R. Sahraeian, Y. Dadmohammadi, B. Shiroud Heidari, J. Seyfi, I. Hejazi, I. Mosleh, A. Abbaspourrad, Nanoperlite effect on thermal, rheological, surface and cellular properties of poly lactic acid/nanoperlite nanocomposites for multipurpose applications, Polym. Test. 91 (2020), 106779, https://doi.org/10.1016/j.polymertesting.2020.106779.

[28] Y. Feng, X. Li, M. Li, D. Ye, Q. Zhang, R. You, W. Xu, Facile preparation of biocompatible silk fibroin/cellulose nanocomposite films with high mechanical performance, ACS Sustain. Chem. Eng. 5 (2017) 6227–6236, https://doi.org/10.1021/acssuschemeng.7b01161.

[29] A. Pae, S.-S. Kim, H.-S. Kim, Y.-H. Woo, Osteoblast-like cell attachment and proliferation on turned, blasted, and anodized titanium surfaces, Int. J. Oral Maxillofac. Implants 26 (2011) 475–481.

[30] B.D. Fairbanks, H. Thissen, G. Maurdev, P. Pasic, J.F. White, L. Meagher, Inhibition of protein and cell attachment on materials generated from N -(2-hydroxypropyl) acrylamide, Biomacromolecules 15 (2014) 3259–3266, https://doi.org/10.1021/bm500654q.

[31] A.B. González-Gil, J.M. Lamo-Espinosa, E. Muiños-López, P. Ripalda-Cemboráin, G. Abizanda, J. Valdés-Fernández, T. López-Martínez, M. Flandes-Iparraguirre, I. Andreu, M.R. Elizalde, K. Stuckensen, J. Groll, E.M. De-Juan-Pardo, F. Prósper, F. Granero-Moltó, Periosteum-derived mesenchymal progenitor cells in engineered implants promote fracture healing in a critical-size defect rat model, J. Tissue Eng. Regen. Med. 13 (2019) 742–752, https://doi.org/10.1002/term.2821.

[32] F. Granero-Moltó, J.A. Weis, M.I. Miga, B. Landis, T.J. Myers, L. O'Rear, L. Longobardi, E.D. Jansen, D.P. Mortlock, A. Spagnoli, Regenerative effects of transplanted mesenchymal stem cells in fracture healing, Stem Cell. 27 (2009) 1887, https://doi.org/10.1002/stem.103. –1898.

[33] E. Muinos-López, P. Ripalda-Cemboráin, T. López-Martínez, A.B. González-Gil, J. M. Lamo-Espinosa, A. Valentí, D.P. Mortlock, J.R. Valentí, F. Prósper, F. Granero-Moltó, Hypoxia and reactive oxygen species homeostasis in mesenchymal progenitor cells define a molecular mechanism for fracture nonunion, Stem Cell. 34 (2016) 2342–2353, https://doi.org/10.1002/stem.2399.

[34] D.W. Grijpma, G.J. Zondervan, A.J. Pennings, High molecular weight copolymers of l-lactide and ε-caprolactone as biodegradable elastomeric implant materials, Polym. Bull. 25 (1991) 327–333, https://doi.org/10.1007/BF00316902.

[35] N. Goonoo, R. Jeetah, A. Bhaw-Luximon, D. Jhurry, Polydioxanone-based bio-materials for tissue engineering and drug/gene delivery applications, Eur. J. Pharm. Biopharm. 97 (2015) 371–391, https://doi.org/10.1016/j.ejpb.2015.05.024.

[36] B.S. Heidari, S.M. Davachi, R. Sahraeian, M. Esfandeh, H. Rashedi, J. Seyfi, Investigating thermal and surface properties of low-density polyethylene/nanoperlite nanocomposites for packaging applications, Polym. Compos. 40 (2019) 2929–2937, https://doi.org/10.1002/pc.25126.

[37] S.M. Davachi, B. Kaffashi, B. Torabinejad, A. Zamanian, In-vitro investigation and hydrolytic degradation of antibacterial nanocomposites based on PLLA/triclosan/nano-hydroxyapatite, Polymer (Guildf). 83 (2016) 101–110.

[38] Y.Q. Zhao, H.Y. Cheung, K.T. Lau, C.L. Xu, D.D. Zhao, H.L. Li, Silkworm silk/poly (lactic acid) biocomposites: dynamic mechanical, thermal and biodegradable properties, Polym. Degrad. Stabil. 95 (2010) 1978–1987, https://doi.org/10.1016/j.polymdegradstab.2010.07.015.

[39] S.M. Davachi, B. Kaffashi, A. Zamanian, B. Torabinejad, Z. Ziaeirad, Investigating composite systems based on poly l-lactide and poly l-lactide/triclosan nanoparticles for tissue engineering and medical applications, Mater. Sci. Eng. C 58 (2016) 294–309, https://doi.org/10.1016/j.msec.2015.08.026.

[40] P.S. Chua, Dynamic mechanical analysis studies of the interphase, Polym. Compos. 8 (1987) 308–313, https://doi.org/10.1002/pc.750080505.

[41] Y.Q. Zhao, H.Y. Cheung, K.T. Lau, C.L. Xu, D.D. Zhao, H.L. Li, Silkworm silk/poly (lactic acid) biocomposites: dynamic mechanical, thermal and biodegradable properties, Polym. Degrad. Stabil. 95 (2010) 1978–1987, https://doi.org/10.1016/j.polymdegradstab.2010.07.015.

[42] X.T. Dong, W.T. Shi, H.C. Dang, W.Y. Bao, X.L. Wang, Y.Z. Wang, Thermal, crystallization properties, and micellization behavior of HEC-g-PPDO copolymer: microstructure parameters effect, Ind. Eng. Chem. Res. 51 (2012) 14037–14046, https://doi.org/10.1021/ie300873a.

[43] B.S. Heidari, V.-S. Cheraghchi, S. Motahari, G.H. Motlagh, S.M. Davachi, Optimized mercapto-modified resorcinol formaldehyde xerogel for adsorption of lead and copper ions from aqueous solutions, J. Sol. Gel Sci. Technol. 88 (2018) 236–248, https://doi.org/10.1007/s10971-018-4782-z.

[44] J. He, Y. Qin, S. Cui, Y. Gao, S. Wang, Structure and properties of novel electrospun tussah silk fibroin/poly(lactic acid) composite nanofibers, J. Mater. Sci. 46 (2011) 2938–2946, https://doi.org/10.1007/s10853-010-5169-x.

[45] H. Zhu, X. Feng, H. Zhang, Y. Guo, J. Zhang, J. Chen, Structural characteristics and properties of silk fibroin/poly (lactic acid) blend films, J. Biomater. Sci. Polym. Ed. 20 (2009) 1259–1274.

[46] Z. Yang, X. Li, J. Si, Z. Cui, K. Peng, Morphological, mechanical and thermal properties of poly(lactic acid) (PLA)/Cellulose nanofibrils (CNF) composites nanofiber for tissue engineering, J. Wuhan Univ. Technol.-Materials Sci. Ed. 34 (2019) 207–215, https://doi.org/10.1007/s11595-019-2037-7.

[47] W. Zhu, X. Zhang, Z. Feng, B. Huang, Effect of ethylene-propylene copolymer with residual PE crystallinity on mechanical properties and morphology of PP/HDPE blends, J. Appl. Polym. Sci. 58 (1995) 551–557, https://doi.org/10.1002/app.1995.070580309.

[48] B. Imre, B. Pukánszky, Compatibilization in bio-based and biodegradable polymer blends, Eur. Polym. J. 49 (2013) 1215–1233, https://doi.org/10.1016/j.eurpolymj.2013.01.019.

[49] F. Wang, H. Wu, V. Venkataraman, X. Hu, Silk fibroin-poly (lactic acid) biocomposites: effect of protein-synthetic polymer interactions and miscibility on material properties and biological responses, Mater. Sci. Eng. C 104 (2019), 109890.

[50] S. Promnil, Y. Ruksakulpiwat, C. Ruksakulpiwat, P.O. Numpaisal, Effect of silk fibroin content on physical and mechanical properties of electrospun poly(lactic acid)/silk fibroin nanofibers for meniscus tissue engineering scaffold, in: J Phys Conf Ser, IOP Publishing, 2022, 12016, https://doi.org/10.1088/1742-6596/2175/1/012016.

[51] Y. Yuan, T.R. Lee, Contact angle and wetting properties, in: Springer Series in Surface Sciences, Springer, 2013, pp. 3–34, https://doi.org/10.1007/978-3-642-34243-1_1.

[52] H.Y. Cheung, K.T. Lau, Y.F. Pow, Y.Q. Zhao, D. Hui, Biodegradation of a silkworm silk/PLA composite, Compos. B Eng. 41 (2010) 223–228, https://doi.org/10.1016/j.compositesb.2009.09.004.

[53] K.G. Grigorov, I.C. Oliveira, H.S. MacIel, M. Massi, M.S. Oliveira, J. Amorim, C. A. Cunha, Optical and morphological properties of N-doped TiO2 thin films, Surf. Sci. 605 (2011) 775–782, https://doi.org/10.1016/j.susc.2011.01.017.

[54] R. Jain, R. Pitchumani, Fractal model for wettability of rough surfaces, Langmuir 33 (2017) 7181–7190, https://doi.org/10.1021/acs.langmuir.7b01524.

[55] M. Dadras Chomachayi, A. Jalali-arani, J.M. Urreaga, The effect of silk fibroin nanoparticles on the morphology, rheology, dynamic mechanical properties, and toughness of poly(lactic acid)/poly(ε-caprolactone) nanocomposite, J. Appl. Polym. Sci. 137 (2020), 49232, https://doi.org/10.1002/app.49232.

[56] M. Mohseni, D.W. Hutmacher, N.J. Castro, Independent evaluation of medical-grade bioresorbable filaments for fused deposition modelling/fused filament fabrication of tissue engineered constructs, Polymers 10 (2018) 40, https://doi.org/10.3390/polym10010040.

[57] M. Mohseni, D.W. Hutmacher, N.J. Castro, Independent evaluation of medical-grade bioresorbable filaments for fused deposition modelling/fused filament fabrication of tissue engineered constructs, Polymers 10 (2018) 40.

[58] C. Guo, C. Li, D.L. Kaplan, Enzymatic degradation of Bombyx mori silk materials: a review, Biomacromolecules 21 (2020) 1678–1686, https://doi.org/10.1021/acs.biomac.0c00090.

[59] M. Byrne, A. Aly, The surgical suture, Aesthetic Surg. J. 39 (2019) S67, https://doi.org/10.1093/asj/sjz036. –S72.

[60] K.K. Yang, X.L. Wang, Y.Z. Wang, Poly(p-dioxanone) and its copolymers, J. Macromol. Sci., Polym. Rev. 42 (2002) 373–398, https://doi.org/10.1081/MC-120006453.

[61] R. You, Y. Xu, G. Liu, Y. Liu, X. Li, M. Li, Regulating the degradation rate of silk fibroin films through changing the genipin crosslinking degree, Polym. Degrad. Stabil. 109 (2014) 226–232, https://doi.org/10.1016/j.polymdegradstab.2014.07.029.

[62] Y. Wang, D.D. Rudym, A. Walsh, L. Abrahamsen, H.J. Kim, H.S. Kim, C. Kirker-Head, D.L. Kaplan, In vivo degradation of three-dimensional silk fibroin scaffolds, Biomaterials 29 (2008) 3415–3428, https://doi.org/10.1016/j.biomaterials.2008.05.002.

[63] N. Bölgen, Y.Z. Menceloğlu, K. Acatay, İ. Vargel, E. Pişkin, In vitro and in vivo degradation of non-woven materials made of poly (ε-caprolactone) nanofibers prepared by electrospinning under different conditions, J Biomater Sci Polym (2005) 1537–1555. Ed. 16.

[64] J. van der Valk, D. Brunner, K. de Smet, Å.F. Svenningsen, P. Honegger, L. E. Knudsen, T. Lindl, J. Noraberg, A. Price, M.L. Scarino, Optimization of chemically defined cell culture media–replacing fetal bovine serum in mammalian in vitro methods, Toxicol. Vitro 24 (2010) 1053–1063.

[65] M.M. Pillai, J. Gopinathan, B. Indumathi, Y.R. Manjoosha, K. Santosh Sahanand, B. K. Dinakar Rai, R. Selvakumar, A. Bhattacharyya, Silk–PVA hybrid nanofibrous scaffolds for enhanced primary human meniscal cell proliferation, J. Membr. Biol. 249 (2016) 813–822.

[66] F. Wang, H. Wu, V. Venkataraman, X. Hu, Silk fibroin-poly (lactic acid) biocomposites: effect of protein-synthetic polymer interactions and miscibility on material properties and biological responses, Mater. Sci. Eng. C 104 (2019), 109890.

[67] K. Hu, Q. Lv, F.Z. Cui, L. Xu, Y.P. Jiao, Y. Wang, Q.L. Feng, H.L. Wang, L.Y. Huang, A novel poly (L-lactide)(PLLA)/fibroin hybrid scaffold to promote hepatocyte viability and decrease macrophage responses, J. Bioact. Compat Polym. 22 (2007) 395–410.

[68] L. Li, H. Li, Y. Qian, X. Li, G.K. Singh, L. Zhong, W. Liu, Y. Lv, K. Cai, L. Yang, Electrospun poly (ε-caprolactone)/silk fibroin core-sheath nanofibers and their potential applications in tissue engineering and drug release, Int. J. Biol. Macromol. 49 (2011) 223–232.

[69] K. Zhang, H. Wang, C. Huang, Y. Su, X. Mo, Y. Ikada, Fabrication of silk fibroin blended P (LLA-CL) nanofibrous scaffolds for tissue engineering, J. Biomed. Mater. Res. Part A: An Official Journal of The Society for Biomaterials, The Japanese Society for Biomaterials, and The Australian Society for Biomaterials and the Korean Society for Biomaterials 93 (2010) 984–993.

[70] L. Chen, C. Yan, Z. Zheng, Functional polymer surfaces for controlling cell behaviors, Mater. Today 21 (2018) 38–59, https://doi.org/10.1016/j.mattod.2017.07.002.

[71] Y. Arima, H. Iwata, Effect of wettability and surface functional groups on protein adsorption and cell adhesion using well-defined mixed self-assembled monolayers, Biomaterials 28 (2007) 3074–3082, https://doi.org/10.1016/j.biomaterials.2007.03.013.

[72] G.H. Altman, R.L. Horan, H.H. Lu, J. Moreau, I. Martin, J.C. Richmond, D. L. Kaplan, Silk matrix for tissue engineered anterior cruciate ligaments, Biomaterials 23 (2002) 4131–4141.

[73] C. Holland, K. Numata, J. Rnjak-Kovacina, F.P. Seib, The biomedical use of silk: past, present, future, Adv. Healthc. Mater. 8 (2019), 1800465.

[74] H. Liu, H. Fan, S.L. Toh, J.C.H. Goh, A comparison of rabbit mesenchymal stem cells and anterior cruciate ligament fibroblasts responses on combined silk scaffolds, Biomaterials 29 (2008) 1443–1453.

[75] A.E. Thurber, F.G. Omenetto, D.L. Kaplan, In vivo bioresponses to silk proteins, Biomaterials 71 (2015) 145–157.

[76] K. Cai, K. Yao, Y. Cui, Z. Yang, X. Li, H. Xie, T. Qing, L. Gao, Influence of different surface modification treatments on poly (D, L-lactic acid) with silk fibroin and their effects on the culture of osteoblast in vitro, Biomaterials 23 (2002) 1603–1611.

[77] K. Cai, K. Yao, S. Lin, Z. Yang, X. Li, H. Xie, T. Qing, L. Gao, Poly (D, L-lactic acid) surfaces modified by silk fibroin: effects on the culture of osteoblast in vitro, Biomaterials 23 (2002) 1153–1160.

[78] C.A. Dinarello, Proinflammatory cytokines, Chest 118 (2000) 503–508.

[79] D. Yang, J. Xiao, B. Wang, L. Li, X. Kong, J. Liao, The immune reaction and degradation fate of scaffold in cartilage/bone tissue engineering, Mater. Sci. Eng. C 104 (2019), 109927.

[80] H. Liu, S.G. Wise, J. Rnjak-Kovacina, D.L. Kaplan, M.M.M. Bilek, A.S. Weiss, J. Fei, S. Bao, Biocompatibility of silk-tropoelastin protein polymers, Biomaterials 35 (2014) 5138–5147.

[81] L. Dizdarević-Hudić, Z. Kušljugić, F. Baraković, S. Brkić, D. Sabitović, E. Jahić, M. Isabegović, E. Smajić, I. Hudić, K. Divković, Correlation between interleukin 6 and interleukin 10 in acute myocardial infarction, Bosn. J. Basic Med. Sci. 9 (2009) 301.

[82] G. Guan, L. Bai, B. Zuo, M. Li, Z. Wu, Y. Li, L. Wang, Promoted dermis healing from full-thickness skin defect by porous silk fibroin scaffolds (PSFSs), Bio Med. Mater. Eng. 20 (2010) 295–308.

[83] D. Yang, Z. Song, J. Shen, H. Song, J. Yang, P. Zhang, Y. Gu, Regenerated silk fibroin (RSF) electrostatic spun fibre composite with polypropylene mesh for reconstruction of abdominal wall defects in a rat model, Artif. Cell Nanomed. Biotechnol. 48 (2020) 425–434.

[84] F.R. Noyes, E.S. Grood, The strength of the anterior cruciate ligament in humans and rhesus monkeys: age related and species related changes, J. Bone Joint Surg. 58 (1976) 1074–1082, https://doi.org/10.2106/00004623-197658080-00006.

[85] E. Francois, D. Dorcemus, S. Nukavarapu, Biomaterials and scaffolds for musculoskeletal tissue engineering, Regen. Eng.Muscoskel. Tissues Interfac. 77 (2015) 3–23, https://doi.org/10.1016/B978-1-78242-301-0.00001-X.

[86] E. Francois, D. Dorcemus, S. Nukavarapu, Biomaterials and scaffolds for musculoskeletal tissue engineering, Regen. Eng.Muscoskel. Tissues Interfac. 77 (2015) 3–23, https://doi.org/10.1016/B978-1-78242-301-0.00001-X.

[87] A. Leroy, B. Nottelet, C. Bony, C. Pinese, B. Charlot, X. Garric, D. Noël, J. Coudane, PLA-poloxamer/poloxamine copolymers for ligament tissue engineering: sound macromolecular design for degradable scaffolds and MSC differentiation, Biomater. Sci. 3 (2015) 617–626, https://doi.org/10.1039/c4bm00433g.